

Redox control on chromium isotope behaviour in silicate melts in contact with magnesiochromite

P. Bonnand, Emilie Bruand, A.K. K Matzen, M. Jerram, Federica Schiavi, B.J. J Wood, M. Boyet, A.N. N Halliday

▶ **To cite this version:**

P. Bonnand, Emilie Bruand, A.K. K Matzen, M. Jerram, Federica Schiavi, et al.. Redox control on chromium isotope behaviour in silicate melts in contact with magnesiochromite. Geochimica et Cosmochimica Acta, 2020, 288 (1), pp.282-300. 10.1016/j.gca.2020.07.038 . hal-02955558

HAL Id: hal-02955558
https://uca.hal.science/hal-02955558

Submitted on 2 Oct 2020

HAL is a multi-disciplinary open access archive for the deposit and dissemination of scientific research documents, whether they are published or not. The documents may come from teaching and research institutions in France or abroad, or from public or private research centers.

L'archive ouverte pluridisciplinaire **HAL**, est destinée au dépôt et à la diffusion de documents scientifiques de niveau recherche, publiés ou non, émanant des établissements d'enseignement et de recherche français ou étrangers, des laboratoires publics ou privés.

Redox control on chromium isotope behaviour in silicate melts in contact with magnesiochromite

P. Bonnand[1,2*], E. Bruand[1,2], A.K. Matzen[2], M. Jerram[2,3], F. Schiavi[1], B.J. Wood[2], M. Boyet[1] and A.N. Halliday[2,3]

[1]Université Clermont Auvergne, CNRS, IRD, OPGC, Laboratoire Magmas et Volcans, F-63000 Clermont-Ferrand, France.

[2]Department of Earth Sciences, University of Oxford, South Parks Road, Oxford, OX1 3AN, United Kingdom.

[3]The Earth Institute, Columbia University, 2910 Broadway, New York, NY 10025 USA.

*Corresponding author

Present address, Université Clermont Auvergne, CNRS, IRD, OPGC, Laboratoire Magmas et Volcans, F-63000 Clermont-Ferrand, France.

Email address: pierre.bonnand@uca.fr

Tel. No: +33 (0)473346783

Abstract:

Transition metal isotopes are particularly useful for understanding the conditions under which magmatic processes occur. Moreover, those with more than one oxidation state (e.g. Cr^{2+}, Cr^{3+} and Cr^{6+}) may also provide powerful constraints on the evolution of the redox state of the mantle over time. By investigating the Cr isotopic compositions in both magnesiochromite and silicate melts during experiments performed at 1300 °C and under controlled redox conditions ($-12 < \log fO_2 < -4$), this study presents the first experimental petro-isotopic investigation of Cr isotope fractionation and reveals clear systematics between Cr concentration, isotopic compositions and fO_2. Two series of experiments were performed to study (a) the dissolution of a natural magnesiochromite into Cr-free silicate melts (series A) and (ii) the crystallisation of magnesiochromite from Cr-doped silicate melts (series B). In agreement with previous studies, the Cr solubility in the silicate melts at equilibrium with magnesiochromite is strongly controlled by oxygen fugacity. Melts produced at low fO_2 are enriched in Cr compared to more oxidised melts. In series A experiments, the Cr isotopic composition of silicate melts are lighter than the initial chromite starting material. The experiments, performed at $-12 < \log fO_2 < -6$, reveal that Cr isotopic compositions of the silicate melts are correlated with fO_2. This demonstrates that, as for the Cr solubility, Cr isotopes are sensitive to fO_2 and could be used to track changes in redox conditions in high-temperature processes. Furthermore, the Cr isotopic compositions of silicate melts that are reacted under more oxidising conditions ($\log fO_2 > -6$) are much lighter than those of melts equilibrated with magnesiochromite at lower oxygen fugacity. The observed variations can be explained by changes in bonding environment for Cr under oxidised conditions in the silicate melts and/or in the magnesiochromite grains. Similarly, the second set of experiments designed to study fractional crystallisation (series B) suggest that Cr isotope fractionation is larger under oxidising conditions.

Keywords: Cr isotopes, Redox conditions, Magnesiochromite, partial melting, fractional crystallisation

1. Introduction

Transition metals are useful for understanding the conditions of differentiation processes such as core formation (e.g. Bourdon et al. 2018). Elements with more than one oxidation state can also provide powerful constraints on the evolution of the redox conditions in the mantle through time (e.g. Williams et al. 2004). The ability to determine isotopic fractionations associated with such differentiation processes has provided new tools whereby early Earth conditions can be explored. Chromium (Cr) is of particular interest because it can be present in two main oxidation states in silicate melts (Cr^{2+} and Cr^{3+}), although during quenching Cr^{2+} is oxidised by Fe^{3+} and only Cr^{3+} has been measured in room-temperature silicate glasses (Berry and O'Neill 2004). Chromium isotopic compositions have been measured in a number of terrestrial and extra-terrestrial samples (e.g. Schoenberg et al. 2008, Moynier et al. 2011, Farkas et al. 2013, Wang et al. 2016, Bonnand et al. 2016a, Bonnand et al. 2016b, Schoenberg et al. 2016, Xia et al. 2017, Bonnand and Halliday 2018, Shen et al. 2018, Shen et al. 2020, Bonnand et al. 2020). However, very little experimental work has been done to independently verify the isotopic effects found in nature. The aim of this study is to investigate the impact of oxygen fugacity on the behaviour of Cr and its isotopic compositions during partial melting and fractional crystallisation in a basaltic system. To this end, the Cr isotopic compositions of silicate melts and chromite have been measured in the run products of 1-atm experiments performed under controlled oxygen fugacity.

2. Background

2.1. Chromium in the mantle and in silicate melts

The Cr concentrations in terrestrial basalts are highly variable and can be up to 2000 µg g^{-1} (e.g. Maclennan et al. 2003). The Cr concentration in mantle peridotites is also variable ranging from 1000 µg g^{-1} to about ~4000 µg g^{-1} (e.g. Bodinier and Godard 2013 and references therein). In basaltic and peridotitic systems, Cr-bearing minerals are spinel, garnet, orthopyroxene and clinopyroxene. During partial melting, Cr is a compatible element meaning that Cr concentrations in the melt are lower than that of the solid residue. The solubility of Cr in the silicate melt is mainly controlled by the partition coefficient between spinel and/or garnet and the silicate melts. The crystal-melt partition coefficient ($D_{crystal\text{-}melt}$) of Cr into spinel (~ 170, Liu and O'Neill 1994) is higher than that of garnet (~ 5.5, McKenzie and O'Nions 1995) and this suggest that melts produced at higher pressure should be enriched in Cr compared to silicate melts produced at low pressure (e.g. Bonnand et al. 2020). During

fractional crystallisation in basaltic systems, Cr is mainly hosted in spinel and clinopyroxene depending on the chemical composition of the silicate melt and the temperature of crystallisation.

The presence of Cr^{2+} in silicate melts has been demonstrated by in-situ XANES measurements, performed by Berry et al. (2006). They also show that the ratio Cr^{2+}/Cr_{TOT} varies with oxygen fugacity and the chemical composition of the silicate melts. The solubility of chromium in silicate melts is dependent on temperature, oxygen fugacity and the chemical composition of the silicate melt (Roeder and Reynolds 1991, Hanson and Jones 1998, Huang et al, 2019). A number of experimental studies have demonstrated that Cr^{2+} is more soluble than Cr^{3+} (e.g. Murck and Campbell 1986). The Cr solubility in silicate melts increases under reduced conditions (from 0.072 Cr_2O_3 wt % at logfO_2 = - 5.1 to 1.43 wt. % at logfO_2 = -12.78, Roeder and Reynolds 1991). This observation is consistent with high Cr concentration in the lunar basalts, compared with their terrestrial counterparts. Chromium solubility also increases with temperature (at logfO_2 = -8, from 0.085 wt % at 1200 ˚C to 0.162 wt. % at 1300 ˚C, Roeder and Reynolds 1991, Hanson and Jones 1998). In silicate melts, Cr^{3+} is octahedrally coordinated whereas Cr^{2+} is located in a distorted octahedral site (Keppler 1992).

2.2. Chromite

In ultramafic and mafic magmatic reservoirs, the main Cr-bearing phases are spinel and pyroxene. There are two types of spinel minerals: 2-3 spinels such as $MgAl_2O_4$ and $MgFe_2^{3+}O_4$ and 2-4 spinels such as Fe_2TiO_4 and the high pressure form of Mg_2SiO_4 (Biagioni and Pasero 2014). Chromite is a 2-3 spinel-structured oxide, common in a variety of rocks such as mantle xenoliths and basalts but also in metamorphic and sedimentary rocks (Dick and Bullen 1984). The 2-3 spinel structure $A^{2+}B^{3+}{}_2O_4$ is based on a nearly ideal cubic close-packed array of oxygen atoms with tetrahedral and octahedral sites. The cations in the tetrahedral sites (A, IV fold coordinated) are usually Mg^{2+}, Fe^{2+}, Zn^{2+}, Mn^{2+}. The cations in the octahedral sites (B, VI fold coordinated) are Al^{3+}, Fe^{3+} and Cr^{3+}. The spinel structure can be modified to accommodate the presence of high Fe^{3+} concentration (e.g. Lenaz and Lughi 2013). In this case the Fe^{3+} can move to the A site and this structure is referred to as inverse spinel. It is commonly assumed however, that magnesiochromite has a normal spinel structure. The normal and inverse structures are two end-members which form a continuum and depending on the chemical composition and the physical conditions, 3+ cations can migrate to the A site. It is important to note, however, that the spinel structure is such that it can host a large number of trace elements including transition metals and high-field-strength elements (HFSE)

(Nielsen et al. 1994). With such high partition coefficients, spinel plays an important role in the trace element budget in most natural igneous rocks, despite relatively low modal proportions. For example, spinel controls the behaviour of many transition metals during partial melting and fractional crystallisation (e.g. Li et al. 1995). Indeed, chromite is often associated with economically important platinum group element (PGE) deposits (Naldrett et al. 2009).

The variations in the chemical compositions of natural chromite has attracted a lot of attention and several parameters are commonly used to describe the observed compositions:

$$Cr\# = Cr^{3+} / (Cr^{3+} + Al^{3+})$$

$$Fe^{3+}\# = Fe^{3+} / (Cr^{3+} + Al^{3+} + Fe^{3+})$$

$$Mg\# = Mg^{2+} / (Mg^{2+} + Fe^{2+})$$

where Cr^{3+}, Al^{3+}, Fe^{3+}, Fe^{2+} and Mg^{2+} are atomic abundances calculated assuming 4 oxygen atoms in the spinel structure and that Cr is only present as Cr^{3+}. In natural spinel, there are large compositional variations between several endmembers and these variations have been linked to the chemical compositions of basalts and/or peridotite, crystallisation temperature, and pressure (e.g. Warren 2016). A number of previous studies have shown that partitioning of transition metals and/or HFSE between spinel/chromite and melts depends on temperature, pressure and the chemical composition of the crystal and melt (Nielsen et al. 1994, Horn et al. 1994, Nielsen and Beard 2000, Blundy and Wood, 2003, Righter et al. 2006, Davis et al. 2017). Redox state also plays a major role in controlling the chemical composition of natural chromite and many experimental studies have calibrated these variations (e.g. Wood et al. 1990, Frost and McCammon, 2008). Although chromite plays a major role in controlling the Cr behaviour in magmatic system, no experimental work has been conducted on the impact of chromite on the behaviour of Cr isotopes.

2.3. Chromium isotopes

The variations in Cr isotopes are reported using the notation:

$$\delta^{53}Cr = \left(\frac{{}^{53}Cr/{}^{52}Cr_{sample}}{{}^{53}Cr/{}^{52}Cr_{NIST\ SRM\ 979}} - 1\right) \times 1000$$

Most recent analyses on mantle xenoliths and mineral separates have shown that Cr isotopes are fractionated during partial melting (Xia et al. 2017, Farkas et al. 2013, Bai et al. 2019). The residues become heavier while partial melting proceeds and the melts are therefore

believed to be lighter than the residues (Xia et al. 2017, Shen et al. 2018). Furthermore, data from mineral separates reveal that, at equilibrium, the Cr isotopic compositions become heavier in the order olivine ≤ cpx = opx < spinel (Shen et al. 2018). It has also been demonstrated that Cr isotopes are fractionated during magmatic differentiation on Earth and on the Moon (Bonnand et al. 2020, Shen et al. in 2020, Bonnand et al. 2016b). Recently, it has been proposed that the isotopic fractionation occurring during fractional crystallisation depends on the the Cr^{3+}/Cr_{TOT} ratios in both the silicate melts and the crystallising phases (Farkas et al. 2013, Schoenberg et al. 2016, Bonnand et al. 2020, Shen et al. 2020). The Cr isotopic variations in HED (Howardite–Eucrite–Diogenite) have also been linked to magmatic processes as well as Cr volatility during planetary accretion (Zhu et al. 2019). Comparing Cr isotope signatures in samples from different planetary bodies is complicated further by the fact that processes active during planet formation may have affected the isotopic compositions of the major reservoirs. For example, the observed difference in Cr isotopes ($\delta^{53}Cr$) between the Moon and the Earth has been attributed to the volatility of Cr during the late stages of the Moon forming Giant Impact (Sossi et al. 2018). In several studies, the variations observed in Cr isotopes in silicate melts and mantle xenoliths have been linked to the isotopic composition of chromite (Farkas et al. 2013, Xia et al. 2017, Shen et al. 2018, Bonnand et al. 2016, Bonnand et al. 2020, Shen et al. 2020). Our ability to estimate the Cr isotopic composition of silicate reservoirs is hampered by our limited understanding of the fractionation factors in high-temperature processes.

3. Analytical methods

3.1. Experiments

The starting compositions used in this study are listed in Table 1. These compositions were synthesised using reagent-grade oxide powders, which were mixed by grinding under ethanol in an agate mortar and pestle.

Two series of experiments were conducted during the course of this study. The first (series A) was designed to study the dissolution of chromite into a Cr-free silicate melt. The second (series B) was designed to study the fractional crystallisation of chromite out of the silicate melts. The only chemical difference between the two silicate melts used in this study is the Cr concentration (see Table 1). The bulk compositions of the melts were chosen such that they were completely molten at 1300°C. To avoid Fe loss from the silicates, loops were pre-saturated by performing multiple saturation experiments (e.g. Hanson and Jones, 1998). We

performed three saturation experiments (72 h per experiment) for each loop at the required temperature and fO_2.

For each series A experiment, 100 mg of starting material A and 5 mg of natural chromite grains (50-200 µm) were combined and pressed into a small pellet (~4 mm diameter). For each series B experiment, 100 mg of starting material B was weighed and pressed into a small pellet. Experimental conditions (e.g. oxygen fugacity, loop material) for each experiment are given in Table 2. Using the series A experimental method, we performed a time series, using a single Pt loop. The loop was used to perform 5 experiments (A3a, A3b, A3c, A3d and A3) with run durations from 2 h to 168 h (Table 2). Between each run, the silicate material was removed and the loop was cleaned in a cold bath of concentrated HF. In addition to the time series, six experiments were performed using method A (A1 to A7), and three experiments were performed using method B (B1 to B3). For each series, the experiment number is given with increasing oxygen fugacity (i.e. A1 is the experiment performed under the more reducing conditions for the series A experiments).

Experiments were performed at the Department of Earth Sciences of the University of Oxford. A schematic is presented in Fig. 1. The experiments were performed by holding the powdered starting material in the hot spots of a gas-mixing furnace (Fig. S1). During the experiments, the temperature was controlled to within ± 5 °C of the desired temperature (1300 °C), and monitored by a thermocouple adjacent to the sample. Oxygen fugacity was controlled using flowing CO and CO_2. Experiments were performed from two log units below to six log units above the Iron-Wüstite (IW) buffer. An O_2 sensor, made of yttria-stabilized zirconia, was used to monitor the oxygen fugacity during the duration of each experiment. The measured fO_2 is thought to be accurate to within 0.1 (1 s.d.) log units. Depending on oxygen fugacity, starting materials were suspended using Pt or Re-loops. The samples for series A experiments were slowly placed into the furnace at 800°C, the temperature was then increased to 1300°C where it was held for 168 h. The experimental procedure was similar for the series B experiments except, in order to facilitate the crystallization of chromite, temperature cycling was employed at the beginning of the experiment. After insertion into the furnace the temperature was increased to 1550 °C, followed by cooling to 1300 °C at 5 °C h^{-1}; the temperature was increased again to 1450 °C followed by cooling to 1300 °C at 5°C h^{-1} after which the temperature was kept constant (at 1300 °C) for 168 h. At the end of all experiments, samples were quenched by dropping them into water.

Previous studies have reported Cr loss during experiments performed both at high and low fO_2 (Hanson and Jones 1998). While Cr loss at low fO_2 is likely due to Cr entering the loop,

Cr volatility was observed in experiments performed in air ($\log fO_2 = -0.68$, Hanson and Jones 1998), an fO_2 that is higher than those used in this study ($\log fO_2$ range from −12 to −4). More recently, Sossi et al. (2019) proposed that Cr is volatile at 1-atm under oxidizing conditions ($\log fO_2 > -7$) at 1300°C. Specifically, they lost almost 80% of their starting Cr after 15 minutes. In contrast, the experiments of Norris and Wood (Norris and Wood, 2017), also conducted at 1300°C and an $\log fO_2$ range of -13 to -7, provide evidence that Cr is not volatile. Our experiments show no clear evidence of Cr loss, either to the loop, or by volatility.

3.2. Sample preparation

Sample preparation for isotope measurements required a different approach between the series A and B experiments. For the A series, the samples retrieved after the experiments were lightly crushed in an agate mortar and pestle and the large chromite grains (>200 µm) were picked from the silicate glass using a binocular stereoscope. Chromite grains were dissolved in a mixture of acids (HNO_3-HCl), using Parr bombs. Despite our best efforts to separate the two phases, a small amount of silicate melt often adhered to the chromite grains. As we show below, this represents a negligible change to the Cr budget of the sample. The silicate melt fractions were first dissolved in cold HF-HNO_3 (3:1) for 24h and then centrifuged to make sure that no chromite grains were present. The samples were then dissolved in 6M HCl to remove the fluorides. For the series B experiments, after crushing in an agate pestle and mortar, the silicate melts were picked under a binocular microscope. The small size of the chromite grains (< 15 µm) meant that it was not possible to effectively separate the chromite grains from the silicate melts by hand. In order to achieve this separation, we performed a sequential leaching of chromite rich sample splits. To this end, the samples were dissolved in cold diluted (3M) HF for 24h. Following this, the samples were then centrifuged for 10 min at 3000 rpm and the supernatant was removed and discarded. The samples were then rinsed with de-ionised water and centrifuged again. The isolated chromite grains were dissolved in acid mixtures (HNO_3-HCl).

For microprobe and Raman spectroscopy analyses, small pieces of each experiment, containing both silicate melts and chromite grains, were picked, mounted in epoxy and polished.

3.3. Microprobe analyses

A Cameca SX5 tactis microprobe and a Cameca SX100 microprobe at the Laboratoire Magmas et Volcans (LMV) were used to determine major-elements composition of the chromites and silicate melts. A 15 kV accelerating voltage, a 15 nA beam current, and a 1 µm electron beam were used. Standards used to calibrate the instrument were Al on Al_2O_3, Mg on MgO, Na on albite, Ti and Mn on $MnTiO_3$, Ca and Si on wollastonite, Fe on Fe_2O_3 and Cr on Cr_2O_3. Cr#, Fe^{3+}# and Mg# presented in this study have been calculated from EPMA analyses by assuming ideal stoichiometry of the spinel phase. Fe^{3+}# and Mg# were calculated by assigning Fe cations either as ferric or ferrous ions to balance negative charge (Stormer 1983). Previous studies have shown that Fe^{3+}/Fe_{TOT} determination using EPMA analyses only, can be affected by large analytical uncertainties (e.g. Wood and Virgo, 1989). Wood and Virgo (1989) provided a robust methodology to correct for this effect using Mössbauer calibrated standards. This technique has been widely used to correct EPMA analyses (e.g. Parkinson and Pearce 1998). Recently, Davis et al. (2017) confirmed that the correction improves accuracy and precision of Fe^{3+}/Fe_{TOT} values if the analysed chromite lies on the mantellic spinel MgO-Cr# correlation. In this study, we have analysed Mössbauer calibrated chromite standards to assess the accuracy of our EMPA methodology (supplementary material). We found that the Fe^{3+}/Fe_{TOT} ratios obtained with our EPMA measurements are in agreement with Mössbauer Fe^{3+}/Fe_{TOT} ratios obtained for the same samples (Wood and Virgo, 1989, Ionov and Wood 1992), which suggests that no correction is needed. Using the standard data, we have determined the analytical uncertainty (2 s.d.) associated with Mg#, Cr# and Fe^{3+}# calculations (± 0.013, ± 0.010 and ± 0.005, respectively).

3.4. Chromium isotope measurements

Protocols for the separation of Cr from silicate matrices have been previously published (e.g. Trinquier et al. 2008; Bonnand et al. 2016a). Only a brief summary is given here: Aliquots of ~2 µg of chromium of the solutions were spiked with the requisite amount of ^{50}Cr-^{54}Cr double spike (Bonnand et al. 2011). The solutions were dried down and taken up in 6M HCl to ensure isotopic equilibrium between the samples and the spike. The protocol used to separate the Cr fraction from the matrix is a two-column procedure (Bonnand et al. 2016a). The first column is designed to remove the major cations while the second column removes the few remaining isobaric interferences, such as Ti. The isotopic measurements were performed on a ThermoFisher Triton TIMS at the University of Oxford and at the LMV. Typical Cr isotope measurements consisted of 54 blocks of 10 cycles. The gains were measured daily and the baselines (30 s) were measured before each block. The amplifier

rotation was used to cancel out the gain differences between each Faraday cup. The reproducibility obtained for the JP-1 reference material over the course of this study is $\delta^{53}Cr$ = -0.108 ± 0.014 ‰ (2 s.d., n = 8) in agreement with previous measurements (Bonnand et al. 2016a, Li et al. 2016, Zhu et al. 2018).

4. Results

4.1. Times series

The chemical compositions of the silicate melts in the time series experiments do not vary except for Cr. The Cr concentration evolves from 0.02 ± 0.03 wt. % after 2 hours to 0.18 ±0.02 wt. % after 120 and 168 hours (Fig. 2). The Cr isotopic compositions (expressed as $\delta^{53}Cr$, relative to NIST SRM 979) of the silicate melts of the time series experiments evolve from -0.167 ± 0.012 ‰ after 24 h to -0.138 ± 0.012 ‰ after 168 h (Fig. 2).

4.2. Silicate melt chemical compositions

4.2.1. Series A

The chemical compositions of the silicate melts of the series A experiments are reported in Table 3. Overall, the variations in major element composition are minor with the exception of FeO in the more reduced experiment (exp A1). The SiO_2, Al_2O_3, MgO and CaO concentrations in the silicate melts are 47.2, 15.4, 11.7 and 17.6 wt. %, respectively. The Cr concentration (Cr_2O_3) in the silicate melts vary from 0.81 to 0.09 wt. %. The Cr concentrations in the silicate melts increase with decreasing oxygen fugacity (Fig. 3).

4.2.2. Series B

The chemical compositions of the silicate melts of the series B experiments are reported in Table 3. There is no variation within the three experiments for all major elements except FeO with exp B1 depleted in FeO compared to exp B2 and B3. The SiO_2, Al_2O_3, MgO and CaO concentrations in the silicate melts are 47.2, 15.2, 11.5 and 18.0 wt. %, respectively. The Cr concentration (Cr_2O_3) in the silicate melts vary from 0.10 ± 0.03 to 0.30 ± 0.06 wt. %. The Cr concentrations in the silicate melts increase with decreasing oxygen fugacity (Fig. 3).

4.3. Chromite chemical composition

4.3.1. Series A

The chemical compositions of the chromite grains in the series A experiments are extremely variable (Figs. 4 and S2). Based on chemical compositions, the series A experiments can be divided into two groups of experiments with similar behaviour. The first group of experiments is composed of exp. A1 to A5 and were performed at $\log fO_2 < -6$. The

chromite grains are chemically heterogeneous in Mg#, Fe^{3+}# and Cr#. Experiments A1 and A2 (logfO_2 –11.9, and –9.6, respectively) are strongly zoned with clear dissolution-reprecipitation textures (Fig. S3). The newly crystallised material at the rim of the crystal is up to 50 microns thick. Experiment A3 (logfO_2 –8.3) has a thin dark rim characterised by a depletion in Fe and enrichments in Cr and Al without obvious dissolution-reprecipitation textures. For the chromites of the first group of samples (A1 to A5), the rims have higher Mg# values and lower Fe^{3+}# and Cr# values compared to the core compositions. The increase in Mg# and decrease in Fe^{3+}# and Cr# values, across experiments, are correlated with oxygen fugacity. As fO_2 decreases, Fe^{3+}# and Cr# decrease.

The second group of experiments is composed of the two most oxidised experiments A6 and A7 (logfO_2 –5.8, and –3.9, respectively). Their chromite grains are chemically homogeneous in Mg# but heterogeneous in Fe^{3+}# with the rims enriched in Fe^{3+} and depleted in Cr compared to the cores (Table 4). Interestingly, A6 and A7 chromites are enriched in Mg relative to Fe^{2+} compared to the starting material compositions (Fig. 4). Overall, all series-A experiments show covariation between log fO_2 and Cr# (and Fe^{3+}#) in the rims of the chromite grains (Fig. 5).

4.3.2. Series B

In this experimental series, chromite grains are euhedral and up to 20 microns in size (Fig. S4). The chemical composition of chromite grains crystallised in the series B experiments are highly heterogeneous (Table 4 and Fig. 6). The three experiments have Mg# values ranging from 0.67 to 0.79. The Fe^{3+}# and Cr# vary from 0 to 0.09 and 0.47 to 0.84, respectively. The core of the bigger chromite grains have generally lower Mg# and Fe^{3+}# and higher Cr# than their rims or the small chromite grains. Differences between B experiments can also be observed, for example, the small (i.e. rims) chromite grains in experiments B1 have systematically lower Fe^{3+}# and Mg# compared to B3 experiment (Fig. 5).

4.4. Chromium isotopic compositions

The Cr isotopic compositions of all silicate melts and chromite grains are given in Table 5. For the silicate melts in series A and B experiments, the δ^{53}Cr values range from -0.449 ± 0.014 to -0.117 ± 0.014 ‰ and from -0.437 ± 0.014 to -0.240 ± 0.014 ‰, respectively. The chromites of the series A experiments have an average δ^{53}Cr value of -0.108 ± 0.014 ‰ (2 s.d., n = 7) within error of the chromite grain added to the starting material (δ^{53}Cr = -0.105 ±

353 0.014 ‰). The starting material used in the series B experiments has a δ^{53}Cr value -0.060 ±
354 0.014 ‰. The chromites from the series B experiments are more heterogeneous with δ^{53}Cr
355 values ranging from 0.063 ± 0.014 to 0.150 ± 0.014 ‰.

356
357 5. Discussion
358 5.1. Chemical and isotopic evolution during the times series experiments

359 The results presented in this study show that the chemical and isotopic compositions of
360 the silicate melts in our experiments vary through time and depend on oxygen fugacity.
361 During the time series experiments the silicate melt compositions are invariant for all the
362 major elements but Cr concentrations vary (Fig. 2). In these experiments, the initial Cr
363 concentration in the melt is ~0 and it gradually increases from ~50 µg g^{-1} after 2 h to 1200 µg
364 g^{-1} after 120 h, as expected from dissolution of the chromite grains into the silicate melts. The
365 fact that the Cr concentration in the melt reaches a plateau after 120 h suggests that the Cr
366 saturation concentration in the melt has been reached, which at 1300 ºC and logfO_2 = -8.6, is
367 approximately 1200 µg g^{-1}.

368 The Cr isotopic compositions of the silicate melts also evolve with time. After 2 hours, the
369 δ^{53}Cr value in the melt is -0.251 ‰ and it rapidly evolves to heavier values after 24 h (-0.167
370 ‰), reaching a plateau after 120 h (-0.143 ‰, Fig. 2). The dissolution of chromite into the
371 silicate melts seems to be driven by a kinetic reaction. Indeed, the first Cr going into the melts
372 is isotopically light compared to the chromite starting material and it evolves toward heavier
373 values with time (Fig. 2). As with the Cr concentrations, it seems that the isotopic
374 composition of the melt reaches steady state after 120-168 h. Due to the slow diffusion rate of
375 Cr^{3+} in the chromite and the resulting zoning observed in chromite of the series A
376 experiments, it is impossible to argue for full isotopic equilibrium in the experimental charge.
377 However, the plateau observed in the time series experiments suggests that the Cr isotopic
378 compositions of the silicate melts are at local equilibrium with the rims of the chromite and
379 we argue that the silicate melts approach Cr isotopic composition equilibrium after 120 h. We
380 therefore decided to run our other experiments for 168 h in order to reach the Cr saturation
381 concentration in the silicate melts and to approach isotopic equilibrium.

382 5.2. Chemical evolution of the silicate melt compositions

383 The chemical composition of the silicate melts in individual experiments and between the
384 experiments of the series A and B are homogeneous, except for Cr. In Figure 3, the Cr
385 concentration in both series of experiments are plotted against oxygen fugacity. The Cr

concentration in the melt increases with decreasing oxygen fugacity (Fig. 3). The two series of experiments lie on the same solubility curve highlighting that, in both cases, the Cr concentration of the melt has closely approached equilibrium with the chromite. Importantly, the increase in Cr solubility in the silicate melts with decreasing fO_2 is in agreement with previous studies that had already shown that Cr is more soluble in silicate melts under reducing conditions (Fig. 2, Roeder and Reynolds 1991; Hanson and Jones 1998).

In a silicate melt, chromium occupies two principal oxidation states, Cr^{2+} and Cr^{3+}. Cr^{2+} is absent from room-temperature silicate glasses due to the oxidation of Cr ($Fe^{3+} + Cr^{2+} \rightarrow Fe^{2+} + Cr^{3+}$) during quenching (Berry et al. 2006). This makes it impossible to measure the Cr^{2+}/Cr^{3+} ratio in our silicate glasses. Hanson and Jones (1998) have proposed a method to calculate the Cr^{2+}/Cr^{3+} ratios in silicate melts in the presence of spinel. The main assumption in this method is that i) at the Ni-NiO oxygen buffer, Cr is only present in Cr^{3+}, and ii) that the Cr^{3+} concentration in the melt is independent of fO_2 (Hanson and Jones 1998). The latter assumption is based on the fact that, in the presence of spinel, the activity of Cr^{3+} ($aCrO_{1.5}$) remains constant and does not vary with fO_2. In order to calculate the Cr^{2+}/Cr^{3+} ratio in our silicate melts, we used the following equation:

$$Cr^{2+}/Cr^{3+} = (Cr_{melt} - Cr_{oxy}) / Cr_{oxy}$$

where Cr_{melt} and Cr_{oxy} are the Cr concentrations in a given experiment and in the most oxidised experiment, respectively. The similarity in composition and experimental conditions between the A and B series means that for the Cr^{2+}/Cr^{3+} calculation, we assume that the Cr^{3+} concentration in our experiments is the average Cr concentration in the experiments performed above the Ni-NiO buffer (A6, A7 and B3). In Figure 7, we report the $log(Cr^{2+}/Cr^{3+})$ versus the *log* of oxygen fugacity for our series of experiments. We obtain a slope of −0.25 ± 0.01 (series A) and −0.27 ± 0.01 (series B) close to the theoretical slope of −0.25 expected for a redox reaction involving a one electron exchange. This is strong evidence that the increase in Cr solubility in our experiments under reducing conditions is controlled by the difference in solubility between Cr^{3+} and Cr^{2+} in silicate melts. This conclusion is in agreement with previous studies on this topic (e.g. Hanson and Jones 1998).

Together with Cr, Fe is another redox sensitive element and the Fe^{3+}/Fe_{TOT} in the silicate melt is also expected to vary with fO_2. We have calculated the Fe^{3+}/Fe_{TOT} ratio in our silicate melts using the calibration given in O'Neill et al. (2018). The results of this calculation are shown in Figure 7b. As expected, given the temperature and the redox conditions in which we

performed our experiments the Fe^{3+}/Fe_{TOT} ratio varies greatly in our silicate melts from 0.02 to 0.45 (Table 3). The amount of Fe^{3+} in the melt varies less than the Cr^{3+}/Cr_{TOT} ratio calculated above because the oxidation reaction for Fe happens at higher fO_2 than that of Cr.

5.3. Chromite chemical evolution

The chromite grains analysed in this study are heterogeneous. The large variations in chemical composition, illustrated by the zoning observed in the chromite from the series A experiments, clearly indicate that the cores of the chromite grains are not at equilibrium with the silicate melts. This can be easily explained by the slow diffusion rate of Cr^{3+} in chromite (Suzuki et al. 2008). However, several systematics in the chromite zoning can be identified (Fig. 4 and S1). For the two most oxidised experiments (exp A6 and A7), the Mg# is homogeneous and higher than the Mg# in the starting material. This observation indicates that, under oxidising conditions, Mg^{2+} and Fe^{2+} diffuse relatively fast and have sufficient time to equilibrate with the melt. In the same experiments, the Fe^{3+}# is higher in the rim than in the cores (Fig. 4). This suggests that the original chromite grain was depleted in Fe^{3+} compared to the chromite at equilibrium with the silicate melts. The trends observed can be explained by diffusion of Fe^{3+} from the melt together with diffusion of Al and Cr from the chromite to the melt.

In the more reduced experiments, the chromite grains are zoned in Mg#, Fe^{3+}# and Cr#. The Mg# is higher in the rims than in the cores (Fig. 4), indicating that the starting material was Fe^{2+} rich compared to the chromite at equilibrium with the silicate melts at different fO_2. This indicates that Fe^{2+} diffuses out of the chromite grain even at low fO_2 but the diffusion rate of Mg^{2+} and Fe^{2+} in the chromite is slower under more reducing conditions. The Mg# in the rims does not correlate with fO_2. The Fe^{3+}# and Cr# are both lower in the rims than in the cores which suggests that the chromite grains are losing Fe and Cr to the melt and/or gaining Al from the melt. This is consistent with a decrease in Fe^{3+}/Fe_{TOT} and Cr^{3+}/Cr_{TOT} in the silicate melts described in the section above. As for the most oxidised experiments, the cores of chromite are not at equilibrium with the silicate melts.

In Figure 4, all chromite data are reported and general trends can be easily seen. First, there is a clear fO_2 control on the rate of diffusion of Fe^{2+} in the chromite grains. Indeed, although all rims tend to have higher Mg# values compared to the starting material, it is clearly the most oxidised experiments that have the highest Mg#. Considering Fe^{3+}# and Cr#, the rims

values are also extremely variable and, overall, the oxidised experiments have higher Fe^{3+}# values compared to the more reduced experiments. The rim chemical compositions are strongly controlled by fO_2 and this is shown in Figure 5. There is a positive correlation between Cr# and Fe^{3+}# in the rim compositions and fO_2. The most reduced experiments have rim Cr# and Fe^{3+}# compositions of 0.5 and 0, respectively. The more oxidised experiments have rim compositions of 0.7 and 0.12. This clearly shows that the composition of the chromite grains in our experiments is controlled by fO_2. Under reducing conditions, Fe^{3+} and Cr^{3+} are lost from the initial chromite. Under more oxidised conditions, Fe^{3+} becomes more stable in the chromite structure and Cr is also favoured. Assuming the rim compositions are in equilibrium with the silicate melts then, this indicates that the partition coefficient of Cr and Fe between chromite and a silicate melt is strongly fO_2 dependent. The D_{Cr} (D_{Cr} = $Cr_{chromite}/Cr_{melt}$) calculated between the rims and the silicate melts in the experiments series A are presented in Figure 8. The D_{Cr} values vary from 55 to 570 and there is a good correlation between D_{Cr} and fO_2. We also present D_{Cr3+} ($D_{Cr3+} = Cr_{chromite}/Cr^{3+}_{melt}$) using the calculations presented in section 5.1. In the series A, the D_{Cr3+} increases with fO_2 (from $\log fO_2 = -12$ to $\log fO_2 = -6$) and then there is a break with smaller D_{Cr3+} values at $\log fO_2 > -6$ (Fig. 8). This suggests that Cr^{3+} becomes less compatible in chromite under oxidising conditions.

In the series B experiments, the chromite grains are also extremely variable. In this study, we have systematically analysed the large and small chromite grains (Fig. 6). Both core and rims were analysed in the large chromite (> 15 µm). The data are presented in Figure 6. The core compositions in all experiments have high Cr_2O_3 concentrations and low Mg#. The rim and small chromites compositions have lower Cr_2O_3 concentrations and higher Mg# (Table 4). This suggests that during fractional crystallisation the chemical composition of the chromite strongly depends on the silicate melt chemical composition. Indeed, the decrease in Cr_2O_3 content in the chromite is controlled by the concentration in the silicate melts while crystallisation proceeds. Interestingly, the Fe^{3+} content in the chromite also evolves with fractional crystallisation but is strongly dependent on the redox conditions of the experiments. This is also true for Cr content but the variations are smaller. Our experiments show that the redox conditions during the experiments control the chemical composition of the crystallising phases. This is best observed in Figure 5, where the Fe^{3+}# and Cr# of the small chromite grains are plotted versus fO_2. The Fe^{3+} content of the chromite increases with increasing fO_2 as observed for the series A chromite. The fact that the chromite grains are chemically heterogeneous indicates that they are not all in equilibrium with the silicate melts. The slow

diffusion of Fe^{3+} and Cr in the chromite lattice means that there is no chemical re-equilibration after the chromites have crystallised out of the silicate melts. This observation provides evidence that the small chromites and rims of the larger grains are more likely to represent the chemical composition of the chromite at equilibrium with the silicate melts. As with the series A experiments, the Cr contents of the small chromite grains were used to calculate partition coefficients (D_{Cr}) which vary from 150 to 390 and are positively correlated with fO_2 (Fig. 8). The partition coefficient values are very similar to the values obtained with the series A experiments. The D_{Cr3+} for the series B experiments are slightly negatively correlated with fO_2 which confirms that under oxidising conditions Cr^{3+} becomes less compatible in chromite. The Fe^{3+}# in the small chromite grains most likely at equilibrium with the silicate melts is correlated with fO_2 (Figure 5). This correlation is very similar to the correlation shown above for the series A experiments. The similarity in Cr concentration, D_{Cr} and Fe^{3+}# of small chromite obtained for the series B experiments and the rims of series A chromite, suggests that although there is not chemical equilibrium between the silicate melts and the entire chromite grains, the rims of the chromite grains are at local equilibrium with the silicate melts.

5.4. Chromium isotope variations

5.4.1. Chromites

The Cr isotopic compositions of the chromites in the series A experiments show little variation. This can be explained by the lack of equilibration between the cores of the chromite grains and the silicate melts, due in large part to the grain size. In this study, the chromites were handpicked from experimental facilitating analysis of single grains. The fact that the reaction rims in the chromite grain are small (relative to the size of the grain) means that Cr isotope measurements of chromite is dominated by the composition of the core. Thus, it is unsurprising that the Cr isotopic compositions of the chromite grains are within error of that of the starting material. This suggests that these compositions are not at equilibrium with the silicate melts and are not discussed further in this manuscript.

5.4.2. Series A

The Cr isotopic compositions of the silicate melts in the series A experiments are lighter than the Cr isotopic composition of the initial chromite added. This suggests that chromite is isotopically heavier than silicate melts, an observation that agrees with both ab-initio calculation and inferences based on lunar and terrestrial samples (Schoenberg et al. 2008, Moynier et al. 2011, Shen et al. 2018, Bonnand et al. 2016, Bonnand et al. 2020, Farkas et al.

2013). In the series A experiments, the Cr isotopic compositions of the silicate melts can be divided into two domains: experiments at log fO_2 above −6, silicate melts have $\delta^{53}Cr$ of approximately −0.45 ‰, while experiments run at logfO_2 below −6, silicate melts have $\delta^{53}Cr$ of approximately −0.15 ‰ (Fig. 9). Additionally, for those experiments run at logfO_2 lower than −6, the Cr isotopic composition of the silicate melts is negatively correlated with the redox conditions and the Cr^{3+}/Cr_{TOT} of the silicate melts (Fig. 10). In these experiments, the Cr isotopic composition in the melts decreases from $\delta^{53}Cr$=−0.12‰ to $\delta^{53}Cr$=−0.15‰ as logfO_2 increases from −12 to −7.

It is possible that the observed variations are controlled by the redox conditions. In this case, the change in isotopic composition could be due to the fact that, at equilibrium, Cr^{2+} and Cr^{3+} in the melts have different isotopic compositions. If this is the case, then we would expect to see $\delta^{53}Cr$ varying with the Cr^{3+}/Cr_{TOT} ratio (and fO_2). It is important to note, however, that the $\delta^{53}Cr$ of silicate melts is lighter with increasing Cr^{3+}/Cr_{TOT}, implying that Cr^{3+} is lighter than Cr^{2+}. Ab-initio calculations suggest the opposite; Cr^{3+} is assumed to be isotopically heavy compared to Cr^{2+} ($\Delta Cr^{3+}\text{-}Cr^{2+} = 0.35*10^6/T^2$, Moynier et al. 2011). In summary, the Cr isotopic composition of silicate melts in contact with magnesiochromite depends on oxygen fugacity. Under reducing conditions, the Cr isotopic composition of the silicate melt is isotopically heavier than silicate melts produced at higher fO_2. This suggests that Cr isotopes could be a powerful tool to study redox conditions in high temperature environments.

Importantly, the two most oxidised experiments have very light Cr isotopic compositions, which could reflect diverse causes. The small Cr concentration in the silicate melts indicates that the amount of chromite dissolving into the melt in oxidised conditions is small and could potentially limit the attainment of local equilibrium between chromite and the silicate melts. It is important to note, however, that the chromite grains in those experiments are the least zoned (although different from the starting composition) which suggests that they have reached equilibrium more rapidly than those under reducing conditions. It is surprising that in the most oxidised conditions, where all Cr is believed to be Cr^{3+}, that the silicate melts exhibit the largest isotopic shifts. Although this observation is consistent with the observation made for more reduced experiments (melts lighter than chromite), the shift in isotopic composition is large, and seemingly abrupt.

Three main mechanisms can be put forward to explain these light values. The Cr isotopic compositions in the silicate melts are controlled by (i) the chemical composition and the

structure of the silicate melt, (ii) the chemical composition and the structure of the chromite grains and (iii) the isotopic fractionation during volatilisation of Cr under high fO_2 conditions. As explained above, depending on the Fe^{3+}/Fe_{TOT} ratio in silicate melt, the Fe^{3+} coordination in the silicate melts vary. In this study, the two most oxidised experiments have Fe^{3+}/Fe_{TOT} ratio > 0.3 and are also characterised by Raman spectra that could indicate a change in coordination number for Fe. There is a possibility that this change in the melt structure might also affect the coordination of Cr^{3+} in the melt. The Cr isotopic shift observed at about $\log fO_2 = -6$ could be the result of a change in Cr^{3+} coordination in the melt. In this case, a change of Cr^{3+} coordination in the melt from VI fold to IV fold could explain the lighter Cr isotopic composition in the silicate melts in oxidising conditions. This suggestion is supported by the changes in the Raman spectra of both experiments performed under oxidizing conditions (Fig. S5). However, it is generally thought that lower coordination number favours heavy isotopes (Young et al. 2015). Alternatively, a change in Cr neighbours in the silicate melt structure could also explain the shift in Cr isotopic composition. A lower force constant in the Cr-O bond could indeed results in lighter Cr isotopic compositions. It is also possible that Cr may be present under Cr^{6+} in the silicate melts above $\log fO_2 = -6$ and this could be responsible for the observed isotopic shifts. Given the fact that Cr undergoes redox changes during quenching, it is very difficult to assess a change in oxidation state and in coordination number.

The second hypothesis is that the chemical composition of the chromite grain controls the observed isotopic shift. In this case, the hypothesis is that under oxidising conditions, Fe^{3+} becomes more compatible in magnesiochromite resulting in a competition between Cr^{3+} and Fe^{3+}. This is supported by the decrease in D_{Cr3+} with fO_2 observed in our experiments (550 to 450 for experiments above and below $\log fO_2 = -6$, respectively). This would suggest that the result of this competition would be a change in the equilibrium fractionation factor between chromite and the silicate melt. In this case, the fractionation factor between chromite and silicate melts is higher under oxidising conditions and would be inversely correlated with D_{Cr}.

Finally, it had been recently argued that Cr is volatile under oxidised conditions (Sossi et al. 2019). The variations in the most oxidised experiments may be caused by loss of isotopically heavy Cr during volatilisation. Our experiments are not designed to quantify the volatility of Cr because the samples after the experiments are not 100% recovered which inhibits mass balance calculation. It is thus difficult to assess whether volatile loss has occurred. The constant flow of gas employed in our experiments means that any evaporative

582 loss will not be at isotopic equilibrium with the silicate melt. Sossi et al. (2019) reported that
583 Cr concentration decreased by ~40% at logfO_2 = −5.6 in 15 minutes at 1300 °C. If
584 volatilisation were the main process controlling the Cr budget in our silicate melts, we would
585 have observed severe depletion in Cr concentration in our experiment performed at logfO_2 =
586 −3.9 and for ~10,000 minutes. Since such depletion did not occur, we consider that volatile
587 loss of Cr is not a significant influence on our results.

588 5.4.3. Series B

589 In the series B experiments, the Cr isotopic measurements of the chromites were made on
590 multi-grain samples, due to the small size (< 10 μm) of the chromites precipitated from the
591 silicate melt. The HCl leaching method used in this study did not selectively sample the small
592 chromite grains but can be regarded as an average composition of chromite in each
593 experiment and not the Cr isotopic composition at equilibrium with the silicate melts.
594 Nevertheless, the Cr isotopic compositions of the chromite in the series B experiments are
595 heavy (by ~0.3 ‰) compared to the Cr isotopic composition of the starting material. This
596 suggests that during fractional crystallisation the chromites are isotopically heavy compared
597 to the silicate melts. This observation is in agreement with the Cr isotopic variations observed
598 in lunar basalt and terrestrial basalts (Bonnand et al. 2016, Bonnand et al. 2020, Shen et al.
599 2020) and also with ab-initio calculations (Moynier et al. 2011) and mineral separates data
600 where chromite is the heaviest of Cr-bearing phases (Shen et al. 2018).

601 The Cr isotopic compositions of the silicate melts in the series B experiments are
602 isotopically light compared to the starting material. Like the series A experiments, the Cr
603 isotopic composition of the melt in the more reduced experiment in series B is also heavier
604 than the isotopic composition of the silicate melts at higher fO_2 (−0.24 and −0.44 at logfO_2 of
605 −10 and −6, respectively; see Fig. 9). Unfortunately, we do not have access to both the melts
606 and the chromite at complete equilibrium. In this series of experiments, the main reaction is
607 fractional crystallisation. We have modelled the Cr isotopic composition of the silicate melts
608 during fractional crystallisation using the initial Cr concentration and isotopic composition of
609 the starting silicate melts. In Figure 11, we show two fractional crystallisation models, one
610 Rayleigh fractionation model and one equilibrium fractionation model. Using this conceptual
611 framework, the isotopic fractionation measured in our experiments represents an average over
612 the entire crystallisation sequence. Two cases can be considered, one in which the isotopic
613 fractionation factor is constant during the entire crystallisation sequence; the second in which
614 it evolves during crystallisation proceeds. In the models presented in Figure 11, the Cr

isotopic compositions of the crystallising chromite is lighter than that measured for the chromite in the series B experiments (Fig. 11). This provides evidence that the fractionation factors vary during crystallisation and are averages from the start of the crystallising sequence to the end. The variation could be linked to the change in the silicate melts chemical composition but also to the change in temperature during the experiments. The results of these models show that experiments B1 and B2 can be explained by a similar ε factor, whereas the most oxidised experiment B3 clearly requires a larger isotopic fractionation between crystallising chromite and the melt. This is in agreement with the observation that under more oxidised conditions the melt is more depleted in heavy isotopes than the melts produced at lower fO_2. This shift in isotopic composition could be linked to the fact that the chemical composition of the chromite grains is controlled by fO_2. The fractionation factor is therefore linked to fO_2 and it is surprising that fractionation factors between chromite and Cr^{3+} in the melt are larger than chromite and Cr^{2+} in the melt. This is difficult to explain with ab-initio calculations because changes in valence state are supposed to lead to higher fractionation factor than changes in bonding environment (Schauble, 2004). In this case, however, it seems that bonding environment in chromite under oxidising conditions strongly favours heavy isotopes. As previously proposed for the series A experiments, the Cr isotopic shift at high fO_2 could be explained by (i) a change in bonding environment in the melts, (ii) a change in bonding environment in the crystallising chromites and (iii) Cr isotopic fractionation during Cr volatilisation under oxidising conditions.

5.5. Implications for Cr isotopes at high temperature

The results of this study can be used to make general comments on Cr isotope behaviour during igneous processes such as partial melting. Our measurements predict that during partial melting, the silicate melts will be enriched in light isotopes, and the residues will be enriched in heavy isotopes. Recent measurements of ocean island basalts (Shen et al. 2020, Bonnand et al. 2020) and in mantle peridotites (Xia et al. 2017, Shen et al. 2018, Bai et al. 2019) show that residues tend to be 0.05 ‰ heavier than products. Furthermore, the results on the time series experiments demonstrate that in non-equilibrium partial melting reactions, Cr isotope fractionations are driven by kinetic reaction and the melts are enriched in light isotopes. Non-equilibrium melting reactions in natural systems would results in enrichment in heavy isotopes in the residues as suggested by Xia et al. (2017). Importantly, our measurements were performed at 1 atmosphere and so the results of these experiments are not directly

transferable to natural systems. The impact of pressure on the Cr isotope behaviour should be studied in order to evaluate this.

The isotopic variations observed in the experiments performed in this study clearly highlight for the first time, the role played by oxygen fugacity in the behaviour of Cr and its isotopes. It seems that fractionations between chromite and silicate melts are larger under oxidising conditions and this possibly could be useful for studying redox reactions in natural systems. This observation, however, is in disagreement with recent data suggesting that during fractional crystallisation, the Cr isotopic fractionation is smaller under oxidising conditions (Shen et al. 2020, Bonnand et al. 2020). Indeed, the observed variations in terrestrial samples for some OIBs can be modelled with fractionation factors ($\Delta^{53}Cr_{crystal\text{-}melts}$) ranging from −0.005 to −0.02 ‰ (Shen et al. 2020, Bonnand et al. 2020). Under more reducing conditions, the fractionation factor used to model the lunar basalts variations is −0.07 ‰. The dichotomy between two recent datasets of natural OIB samples and our experiments suggest that either chromite is not controlling the Cr budget during fractional crystallisation of OIB samples or that other physical parameters play a role in controlling Cr isotope fractionation. Our study clearly shows that a better understanding of Cr isotopes behaviour in high temperature systems is needed.

6. Conclusions

We have investigated the variations in chemical composition and Cr isotopic compositions in both magnesiochromite and silicate melts during experiments performed under controlled redox conditions. Two series of experiments were performed to study both dissolution (series A) and crystallisation (series B) reactions.

Overall, the chemical composition of the silicate melts is relatively constant with the exception of Cr. As expected, the Cr solubility in silicate melts in our experiments is controlled by temperature and oxygen fugacity. We confirm that chromium becomes more soluble under reducing conditions. The chemical compositions of the chromite in the dissolution experiments (series A) are extremely variable as demonstrated by their zoning in each experiment. The Fe^{3+}# in the rims correlates with fO_2 and this indicates that the chemical composition of the chromites are controlled by fO_2. The partition coefficient of Cr between chromite and silicate melts vary with fO_2; DCr is positively correlated with fO_2 and DCr^{3+} is

680 weakly negatively correlated. This indicates that Cr^{3+} becomes less compatible in chromite
681 under oxidising conditions because of the competition with Fe^{3+}. In the series B experiments,
682 the chromite grains are heterogeneous and several processes play a role in the observed
683 chemical evolution: the redox conditions, the temperature and the chemical composition of
684 the evolving silicate melts. Raman spectroscopy was used to analyse both silicate melts
685 (series A and B) and in chromite (series B only). In summary, the Raman spectra are strongly
686 influenced by the presence of Fe^{3+} in both the melts and the chromite grains. The changes in
687 the Raman spectra do not allow us to definitively show a change in Fe^{3+} coordination in the
688 silicate melts. However, the differences in Raman spectra clearly indicate that the experiments
689 performed under oxidising conditions are structurally distinct from the experiments performed
690 under reducing conditions.

691 The Cr isotopic compositions measured in the silicate melts in both series A and B
692 experiments are strongly influenced by oxygen fugacity. The Cr isotopic composition of the
693 silicate melts in the experiments from the series A group performed at $\log fO_2 < -6$ are
694 correlated with fO_2. This suggests that Cr isotopes is a powerful tool to study changes in redox
695 conditions in high temperature processes. The Cr isotopic composition of the silicate
696 performed under more oxidising conditions are isotopically much lighter. Two main factors
697 (not mutually exclusive) are proposed to explain such variations: (i) a change in Cr bonding
698 environment in the silicate melt (ii) a change in Cr bonding environment in the chromite.
699 More work is needed to definitively determine the factors that control the isotopic behaviour
700 of Cr in silicate melts. Finally, the Cr isotopic composition for the series B experiments
701 indicate that Cr isotopes are fractionated during fractional crystallisation of magnesiochromite
702 from silicate melts. As also shown in the series A experiments, it seems that the fractionation
703 factor is higher under oxidised conditions. Our work also shows that it is likely that the
704 fractionation factor during fractional crystallisation varies with the chemical composition of
705 the chromites, the chemical composition of the silicate melts and temperature. These factors,
706 in addition to the fO_2, likely play a major role in controlling Cr isotope behaviour in igneous
707 processes.

708

709

710

711

Acknowledgments:

This research was supported by STFC grant (ST/M001318/1) to ANH and BJW. M.B. acknowledge support from the European Union's Horizon 2020 research and innovation programme (grant agreement no 682778). We thank J.-L. Devidal for assistance with microprobe analyses and D. Smythe for numerous discussions. We would like to thank Ronny Schoenberg and two anonymous reviewers for their helpful comments.

Declaration of competing interest:

We have no competing financial interests or personal relationship that could have appeared to influence the work reported in this paper.

References:

Bai Y., Su B.X., Xiao Y., Chen C., Cui M.M., He X.Q., Qin L.P., Charlier B., (2019) Diffusion-driven chromium isotope fractionation in ultramafic cumulate minerals: Elemental and isotopic evidence from the Stillwater Complex. *Geochim. Cosmochim. Acta* **263**, 167–181. https://doi.org/10.1016/j.gca.2019.07.052

Berry A. J. and O'Neill H. S. C., (2004) A XANES determination of the oxidation state of chromium in silicate glasses. *Am. Mineral.* **89**, 790–798.

Berry A. J., O'Neill H. S. C., Scott D. R., Foran G. J., Shelley J. M. G., (2006) The effect of composition on Cr2+/Cr3+ in silicate melts. *Am. Mineral.* **91**, 1901–1908. https://doi.org/10.2138/am.2006.2097

Biagioni C. and Pasero M. (2014) The systematics of the spinel-type minerals: An overview *Am. Mineral.* **99**, 1254–1264.

Blundy J. and Wood B. (2003) Partitioning of trace elements between crystals and melts. *Earth Planet. Sci. Lett.* **210**, 383–397. https://doi.org/10.1016/S0012-821X(03)00129-8

Bodinier J. L. and Godard M. (2013) Orogenic, Ophiolitic, and Abyssal Peridotites, 3rd ed, *Treatise on Geochemistry*: Second Edition. Elsevier Ltd. https://doi.org/10.1016/B978-0-08-095975-7.00204-7

Bonnand P. and Halliday A.N. (2018) Oxidized conditions in iron meteorite parent bodies. *Nat. Geosci.* **11**, 401-405. https://doi.org/10.1038/s41561-018-0128-2

Bonnand P., Parkinson I. J., James R. H., Karjalainen A.-M., Fehr M. A. (2011) Accurate and precise determination of stable Cr isotope compositions in carbonates by double spike MC-ICP-MS. *J. Anal. At. Spectrom.* **26**, 528–535. https://doi.org/10.1039/c0ja00167h

Bonnand P., Parkinson I. J., Anand M. (2016a) Mass dependent fractionation of stable chromium isotopes in mare basalts: Implications for the formation and the differentiation of the Moon. *Geochim. Cosmochim. Acta* **175**, 208–221. https://doi.org/10.1016/j.gca.2015.11.041

Bonnand P., Williams H. M., Parkinson I. J., Wood B. J., Halliday A. N. (2016b) Stable chromium isotopic composition of meteorites and metal-silicate experiments: Implications for fractionation during core formation. *Earth Planet. Sci. Lett.* **435**, 14–21. https://doi.org/10.1016/j.epsl.2015.11.026

Bonnand P., Doucelance R., Boyet M., Bachèlery P., Bosq C., Auclair D., Schiano P., (2020) The influence of igneous processes on the chromium isotopic compositions of terrestrial basalts. *Earth Planet. Sci. Lett.* **532**, 116028. https://doi.org/10.1016/j.epsl.2019.116028

Bourdon B., Roskosz M., Hin R. C. (2018) Isotope tracers of core formation. *Earth-Science Rev.* **181**, 61–81. https://doi.org/10.1016/j.earscirev.2018.04.006

Davis F. A., Cottrell E., Birner S. K., Warren J. M., Lopez O. G. (2017) Revisiting the electron microprobe method of spinel-olivine-orthopyroxene oxybarometry applied to spinel peridotites. *Am. Mineral.* **102**, 421–435. https://doi.org/10.2138/am-2017-5823

Dick H. J. B. and Bullen T., (1984) Chromian spinel as a petrogenetic indicator in abyssal and alpine-type peridotites and spatially associated lavas. *Contrib. to Mineral. Petrol.* **86**, 54–76. https://doi.org/10.1007/BF00373711

Farkas J., Chrastny V., Novak M., Cadkova E., Pasava J., Chakrabarti R., Jacobsen S. B., Ackerman L., Bullen T. D. (2013) Chromium isotope variations (delta Cr-53/52) in mantle-derived sources and their weathering products: Implications for environmental studies and the evolution of delta Cr-53/52

781 in the Earth's mantle over geologic time. *Geochim. Cosmochim. Acta* **123**, 74–92.
782 https://doi.org/10.1016/j.gca.2013.08.016

783 Frost D. J. and McCammon C. A. (2008). The Redox State of Earth's Mantle. *Annu. Rev. Earth*
784 *Planet. Sci.* **36**, 389–420. https://doi.org/10.1146/annurev.earth.36.031207.124322

785 Hanson B. and Jones J. H. (1998). The systematics of Cr3+ and Cr2+ partitioning between olivine and
786 liquid in the presence of spinel. *Am. Mineral.* **83**, 669–684.

787 Horn I., Foley S. F., Jackson S. E., Jenner G. A. (1994). Experimentally determined partitioning of
788 high field strength- and selected transition elements between spinel and basaltic melt. *Chem. Geol.*
789 **117**, 193–218. https://doi.org/10.1016/0009-2541(94)90128-7

790 Huang J., Hao J., Huang F., Sverjensky D.A. (2019), Mobility of chromium in high temperature
791 crustal and upper mantle fluids; Geochemical Perspective Letters. 2019, Vol, 12, p. 1-6.

792 Ionov D. A. and Wood B. J. (1992) The oxidation state of subcontinental mantle: oxygen
793 thermobarometry of mantle xenoliths from central Asia. *Contrib. to Mineral. Petrol.* **111**, 179–193.
794 https://doi.org/10.1007/BF00348950

795 Keppler H. (1992) Crystal field spectra and geochemistry of transition metal ions in silicate melts and
796 glasses. *Am. Mineral.* **77**, 62–75.

797 Khedim H., Podor R., Rapin C., Vilasi M. (2008) Redox-control solubility of chromium oxide in soda-
798 silicate melts. *J. Am. Ceram. Soc.* **91**, 3571–3579. https://doi.org/10.1111/j.1551-2916.2008.02692.x

799 Li C. F., Feng L. J., Wang X. C., Chu Z. Y., Guo J. H., Wilde S. A, (2016) Precise measurement of Cr
800 isotope ratios using a highly sensitive Nb2O5 emitter by thermal ionization mass spectrometry and an
801 improved procedure for separating Cr from geological materials. *J. Anal. At. Spectrom.* 31, 2375–
802 2383. https://doi.org/10.1039/c6ja00265j

803 Li J.-P., O'Neill H., Seifert F. (1995). Subsolidus Phase Relations in the System MgO-SiO 2-Ci^O in
804 Equilibrium with Metallic Cr, and their Significance for the Petrochemistry of Chromium Subsolidus
805 phase relations have been determined in the systems. *J. Petrol.* **36**, 107–133.

806 Liu, X. and O'Neill, H. S. C. (2004) The effect of Cr2O3 on the partial melting of spinel
807 lherzolite in the system CaO-MgO-Al2O3-SiO2-Cr2O3 at 1.1 GPa. *J. Petrol.* **45**, 2261–2286.
808 https://doi .org /10 .1093 /petrology /egh055.

809 Maclennan J., McKenzie D., Hilton F., Gronvold K., Shimizu N. (2003) Geochemical variability in a
810 single flow from northern Iceland. *J. Geophys. Res.* Earth **108**. https://doi.org/10.1029/2000JB000142

811 McKenzie, D. and O'Nions, R. K. (1995). The source regions of ocean island basalts. *J.*
812 *Petrol.* **36**, 133–159. https://doi .org /10 .1093 /petrology /36 .1

813 Moynier F., Yin Q.-Z., Schauble E. (2011) Isotopic Evidence of Cr Partitioning into Earth's Core.
814 *Science* **331**, 1417–1420. https://doi.org/10.1126/science.1199597

815 Murck B. W. and Campbell I. H. (1986) The effects of temperature, oxygen fugacity and melt
816 composition on the behaviour of chromium in basic and ultrabasic melts. *Geochim. Cosmochim. Acta*
817 **50**, 1871–1887. https://doi.org/10.1016/0016-7037(86)90245-0

818 Naldrett A. J., Wilson A., Kinnaird J., Chunnett G. (2009) PGE tenor and metal ratios within and
819 below the Merensky Reef, Bushveld Complex: Implications for its genesis. *J. Petrol.* **50**, 625–659.
820 https://doi.org/10.1093/petrology/egp015

Nebel O., Campbell I. H., Sossi P. A., Van Kranendonk M. J. (2014) Hafnium and iron isotopes in early Archean komatiites record a plume-driven convection cycle in the Hadean Earth. *Earth Planet. Sci. Lett.* **397**, 111–120. https://doi.org/10.1016/j.epsl.2014.04.028

Nielsen R. L. and Beard J. S. (2000) Magnetite – melt HFSE partitioning. *Chem. Geol.* **164**, 21–34.

Nielsen R. L., Forsythe L. M., Gallahan W. E., Fisk M. R. (1994) Major- and trace-element magnetite-melt equilibria. *Chem. Geol.* **117**, 167–191.

Norris C. A., Wood B. J. (2017) Earth's volatile contents established by melting and vaporization. *Nature* **549**, 507–510. https://doi.org/10.1038/nature23645

O'Neill H. S. C., Berry A. J., Mallmann G. (2018) The oxidation state of iron in Mid-Ocean Ridge Basaltic (MORB) glasses: Implications for their petrogenesis and oxygen fugacities. *Earth Planet. Sci. Lett.* **504**, 152–162. https://doi.org/10.1016/j.epsl.2018.10.002

Parkinson I. J. and Pearce J. A. (1998) Peridotites from the Izu-Bonin-Mariana forearc (ODP Leg 125): evidence for mantle melting and melt-mantle interaction in a supra-subduction zone setting. *J. Petrol.* **39**, 1577–1618. https://doi.org/10.1093/petroj/39.9.1577

Roeder P. L. and Reynolds I. (1991) Crystallisation of chromite and chromium solubility in basaltic melts. *J. Petrol.* **32**, 909–934. https://doi.org/10.1093/petrology/32.5.909

Schauble E. A. (2004) Applying Stable Isotope Fractionation Theory to New Systems. Reviews in Mineralogy & Geochemistry, **55**, 65-111.

Schoenberg R., Merdian A., Holmden C., Kleinhanns I. C., Hassler K., Wille M., Reitter E. (2016) The stable Cr isotopic compositions of chondrites and silicate planetary reservoirs. *Geochim. Cosmochim. Acta* **183**, 14–30. https://doi.org/10.1016/j.gca.2016.03.013

Schoenberg R., Zink S., Staubwasser M., von Blanckenburg F. (2008) The stable Cr isotope inventory of solid Earth reservoirs determined by double spike MC-ICP-MS. *Chem. Geol.* **249**, 294–306. https://doi.org/10.1016/j.chemgeo.2008.01.009

Shen J., Qin L., Fang Z., Zhang Y., Liu J., Liu W., Wang F., Xiao Y., Yu H., Wei S. (2018) High-temperature inter-mineral Cr isotope fractionation: A comparison of ionic model predictions and experimental investigations of mantle xenoliths from the North China Craton. *Earth Planet. Sci. Lett.* **499**, 278–290. https://doi.org/10.1016/j.epsl.2018.07.041

Shen, J., Xia, J., Qin, L., Carlson, R. W., Huang, S., Helz, R. T., Mock, T. D. (2020) Stable chromium isotope fractionation during magmatic differentiation: Insights from Hawaiian basalts and implications for planetary redox conditions. *Geochim. Cosmochim. Acta*. **278**, 289-304. https://doi.org/10.1016/j.gca.2019.10.003

Sossi P. A., Moynier F., van Zuilen K. (2018) Volatile loss following cooling and accretion of the Moon revealed by chromium isotopes. *Proc. Natl. Acad. Sci.* U. S. A. **115**, 10920–10925. https://doi.org/10.1073/pnas.1809060115

Sossi P. A., Klemme S., O'Neill H. S. C., Berndt J., Moynier F. (2019) Evaporation of moderately volatile elements from silicate melts: experiments and theory. *Geochim. Cosmochim. Acta* **260**, 204–231. https://doi.org/10.1016/j.gca.2019.06.021

Stormer, J. C., (1983) The effects of recalculation on estimates of temperature and oxygen fugacity from analyses of multicomponent iron-titanium oxides. Am. Mineral. **68**, 586–594.

Suzuki A. M., Yasuda A., Ozawa K. (2008) Cr and Al diffusion in chromite spinel: Experimental determination and its implication for diffusion creep. *Phys. Chem. Miner.* **35**, 433–445. https://doi.org/10.1007/s00269-008-0238-2

Trinquier A., Birck J. L., Allègre C. J. (2008) High-precision analysis of chromium isotopes in terrestrial and meteorite samples by thermal ionization mass spectrometry. *J. Anal. At. Spectrom.* **23**, 1565–1574. https://doi.org/10.1039/b809755k

Warren J. M. (2016) Global variations in abyssal peridotite compositions. *Lithos* **248**, 193–219. https://doi.org/10.1016/j.lithos.2015.12.023

Williams H. M., McCammon C. A., Peslier A. H., Halliday A. N., Teutsch N., Levasseur S., Burg J. P. (2004) Iron isotope fractionation and the oxygen fugacity of the mantle. *Science* **304**, 1656–1659. https://doi.org/10.1126/science.1095679

Wood B. J., Virgo D. (1989) Upper mantle oxidation state: Ferric iron contents of Iherzolite spinels by 57Fe Mössbauer spectroscopy and resultant oxygen fugacities. *Geochim. Cosmochim. Acta* **53**, 1277–1291. https://doi.org/10.1016/0016-7037(89)90062-8

Wood B. J., Bryndzia L. T., Johnson K.E. (1990) Mantle oxidation state and its relationship to tectonic environment and fluid speciation. *Science*, **248**, 337–345.

Xia J., Qin L., Shen J., Carlson R. W., Ionov D. A., Mock T. D. (2017) Chromium isotope heterogeneity in the mantle. *Earth Planet. Sci. Lett.* **464**, 103–115. https://doi.org/10.1016/j.epsl.2017.01.045

Young E. D., Manning C. E., Schauble E. A., Shahar A., Macris C. A., Lazar C., Jordan M. (2015) High-temperature equilibrium isotope fractionation of non-traditional stable isotopes: Experiments, theory, and applications. *Chem. Geol.* **395**, 176–195. https://doi.org/10.1016/j.chemgeo.2014.12.013

Zhu J. M., Wu G., Wang X., Han G., Zhang L. (2018) An improved method of Cr purification for high precision measurement of Cr isotopes by double spike MC-ICP-MS. *J. Anal. At. Spectrom.* **33**, 809–821. https://doi.org/10.1039/c8ja00033f

Zhu, K., Sossi, P.A., Siebert, J., Moynier, F., Tracking the volatile and magmatic history of Vesta from chromium stable isotope variations in eucrite and diogenite meteorites. *Geochim. Cosmochim. Acta* 266, 2019, 598–610, https://doi.org/10.1016/j.gca.2019.07.043.

Figure captions:

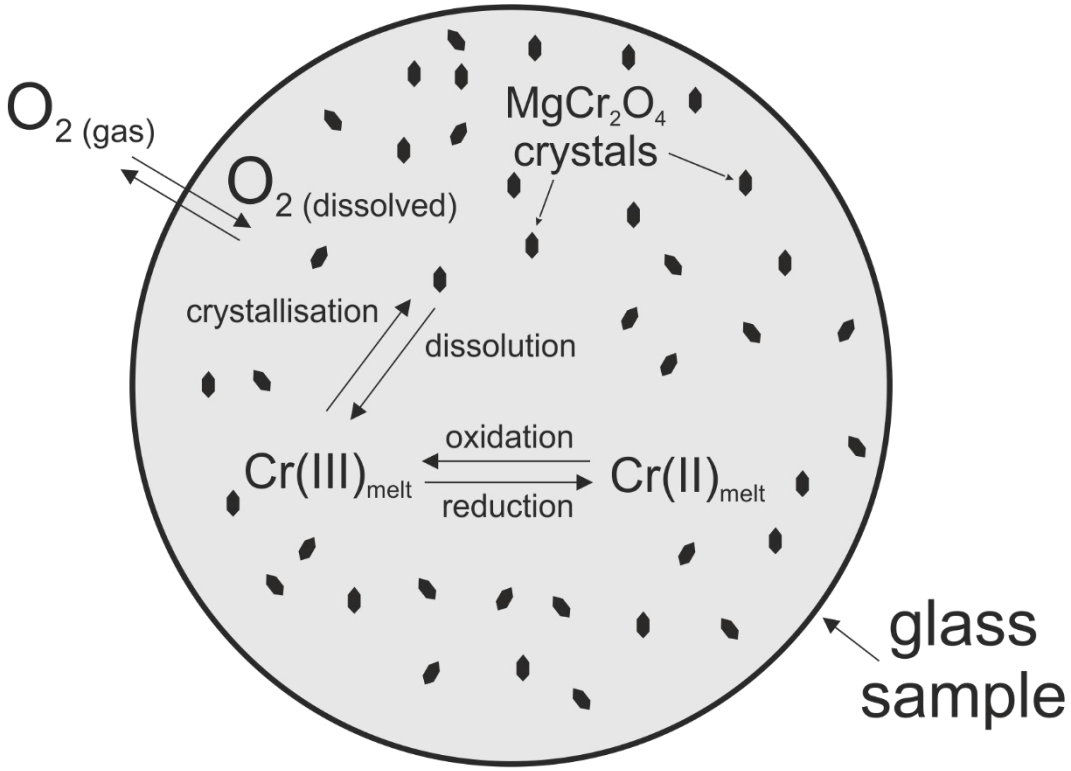


Figure 1: Schematic description of the reactions occurring during the experiments performed in this study. In the series A experiments, the magnesiochromite dissolve as Cr^{3+} in the silicate melts and depending on the redox conditions are reduced to Cr^{2+}. In the series B experiments, the magnesiochromite crystallised from the silicate melts. Figure modified from Khedim et al. (2008).

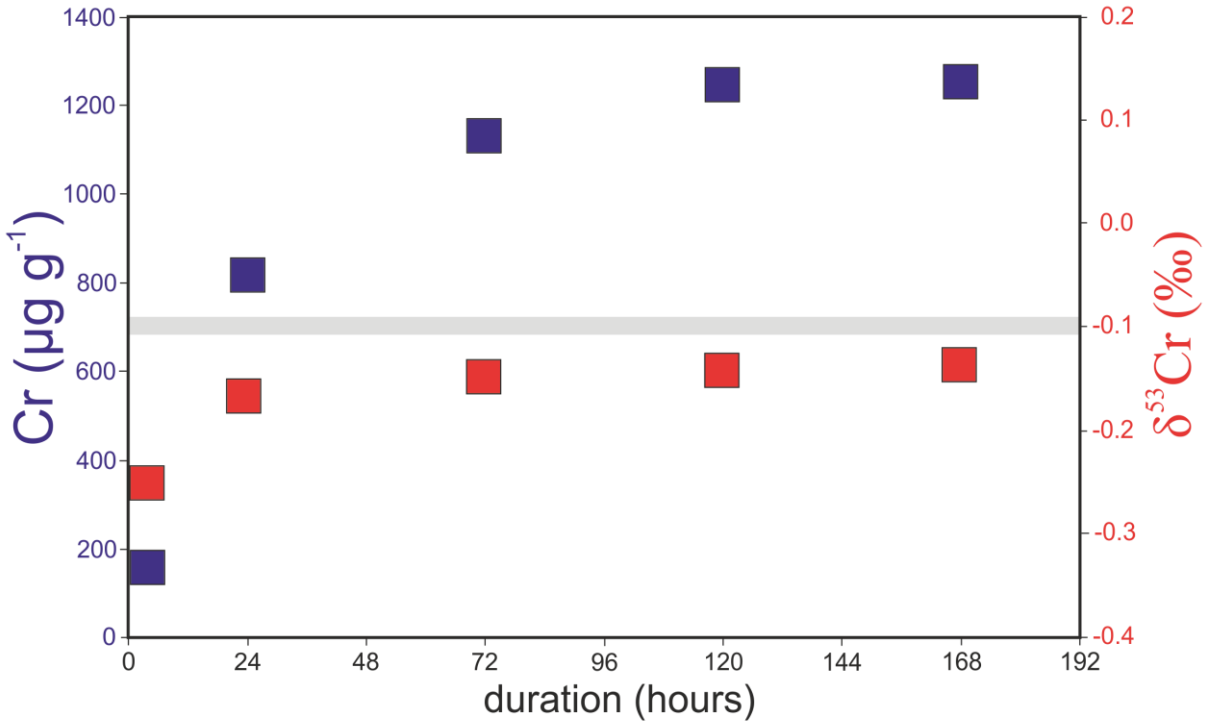
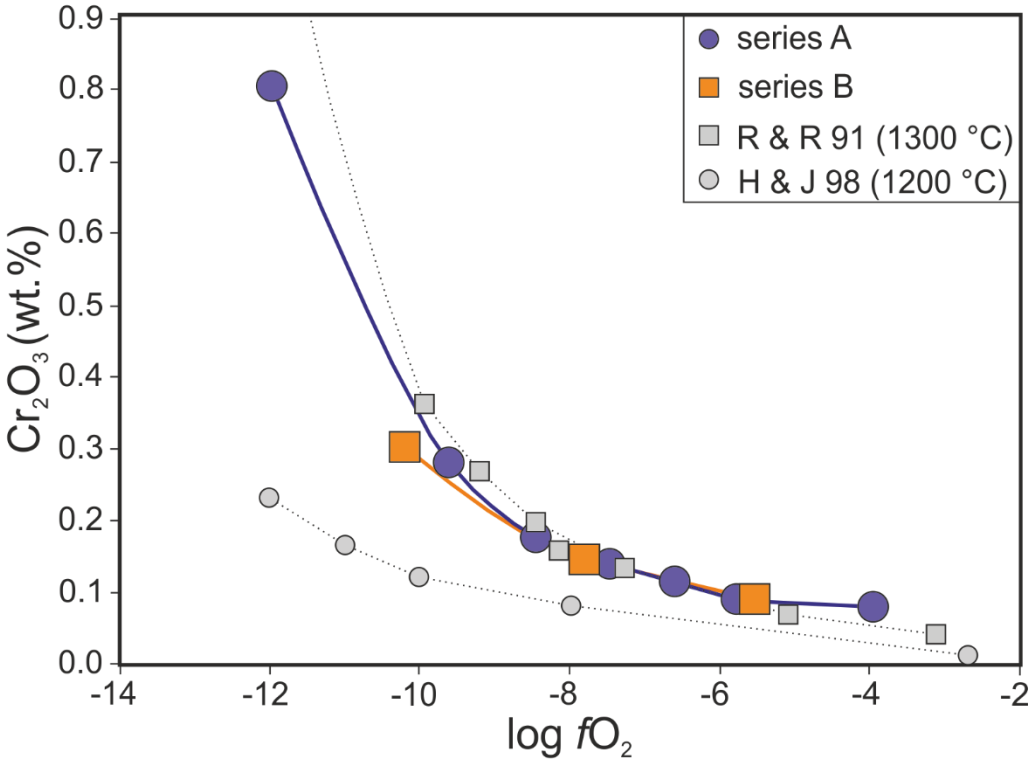


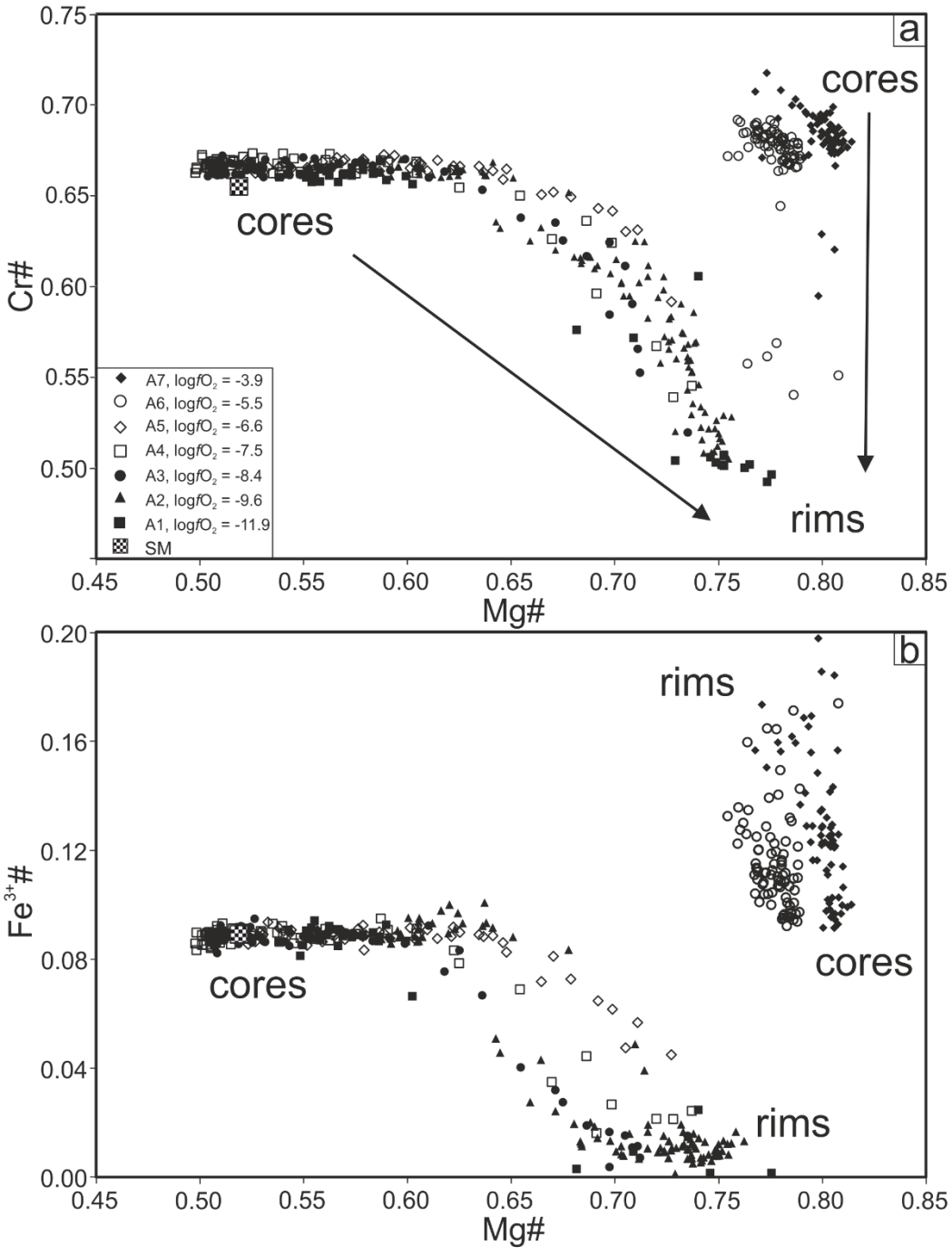
Figure 2: Chromium concentrations in the silicate melts versus time. The experiments shown in this figure form part of the time series experiments (A3, A3a, A3b, A3c and A3d). The grey horizontal bar is the Cr isotopic composition of the chromite at the start of the time series experiments. The blue and red squares are the Cr concentration and Cr isotopic composition in the silicate melt of the time series experiments, respectively.



911

912 **Figure 3**: Cr chemical compositions in the silicate melts of series A and B experiments. The grey and

913 yellow data in (a) are from Roeder and Reynolds (1991) and Hanson and Jones (1998), respectively.



914

915 **Figure 4**: Cr# (a) and Fe^{3+}# (b) for the chromite in the series A experiments. The checkered square is
916 the composition of the starting material (SM). Note that the most oxidised experiments produced rims
917 substantially poorer in Cr and richer in Fe^{3+} than the cores.

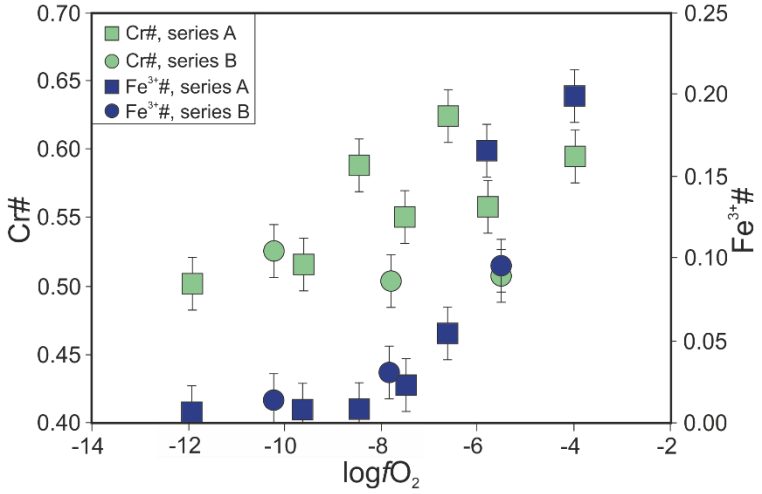
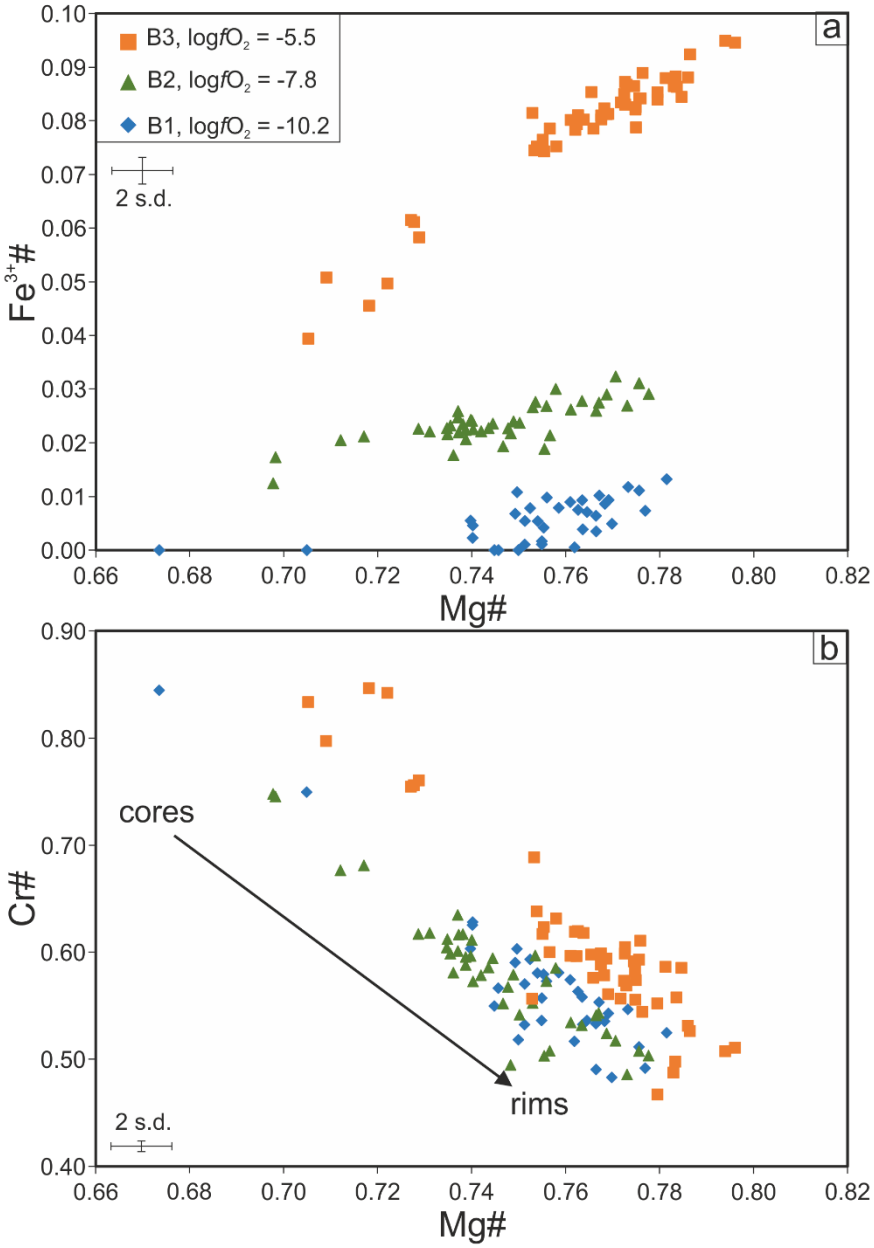
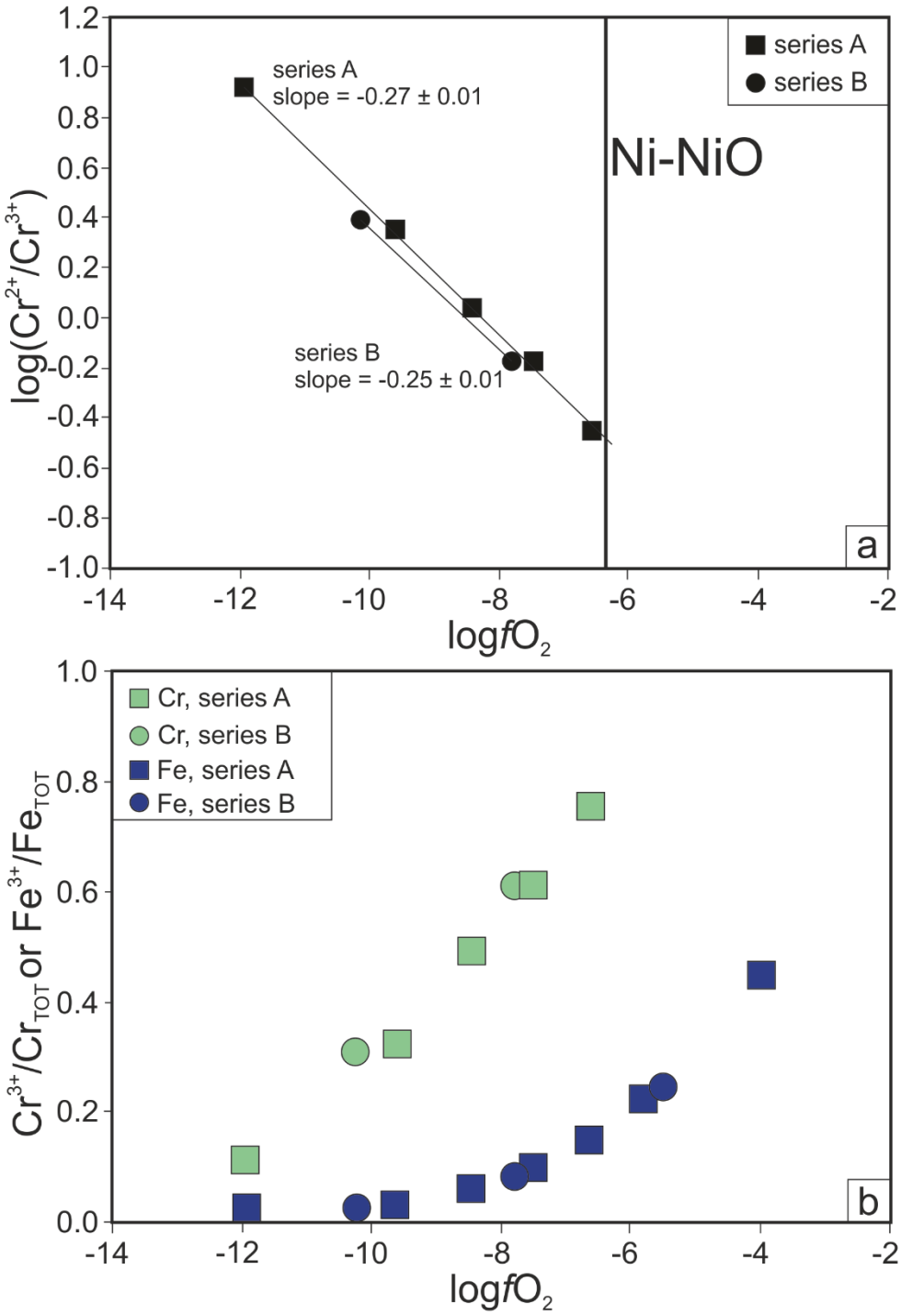


Figure 5: Cr number (green) and Fe^{3+}# (blue) in the rim (or small) chromite versus oxygen fugacity.



920

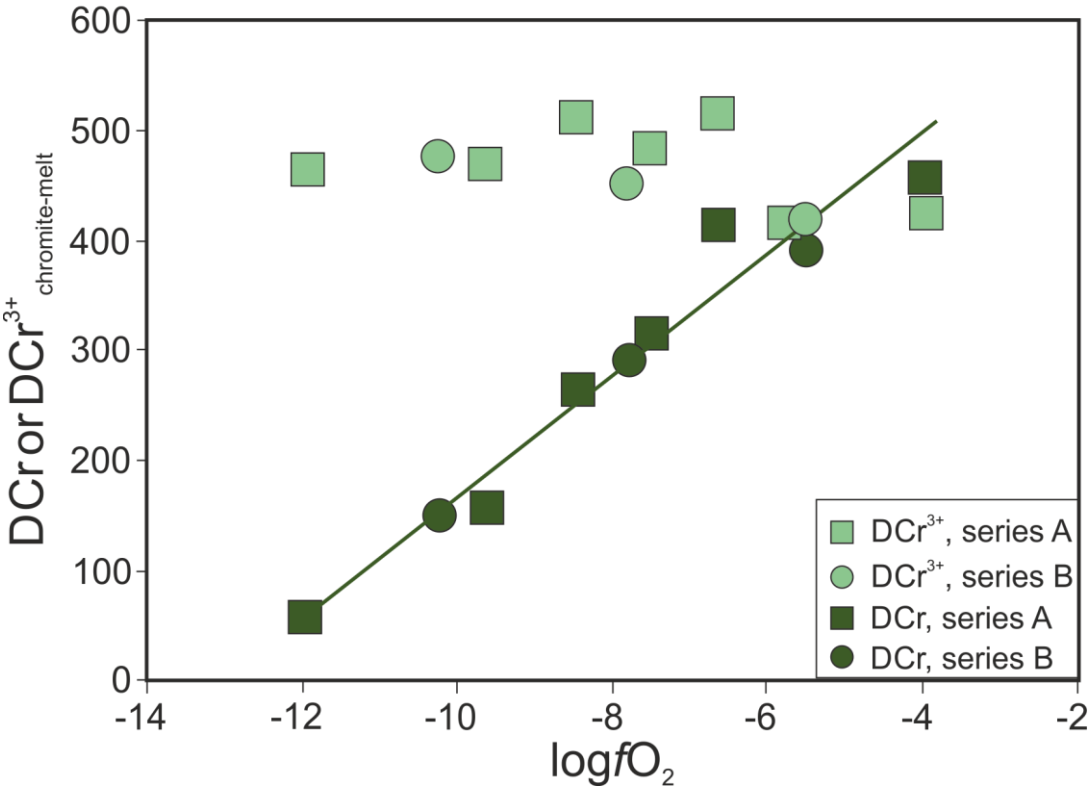
921 **Figure 6**: Fe^{3+}# (a) and Cr# (b) for the chromite in the series B experiments.



922

923 **Figure 7**: *Log*(Cr^{2+}/Cr^{3+}) (a) and Cr^{3+}/Cr_{TOT} (b) in the silicate melts versus *log* of oxygen fugacity. In

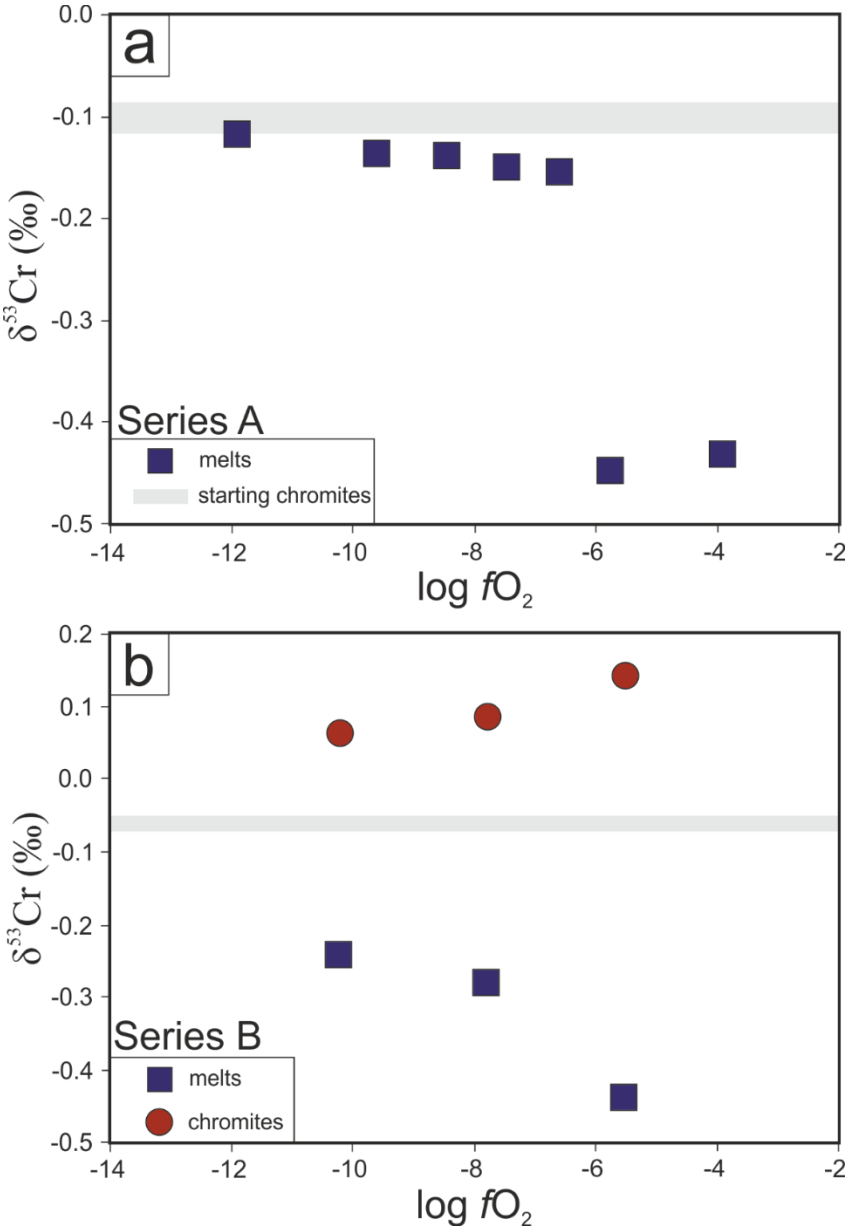
924 (b), in blue, Fe^{3+}/Fe_{TOT} in the silicate melts calculated with O'Neill (2018).



925

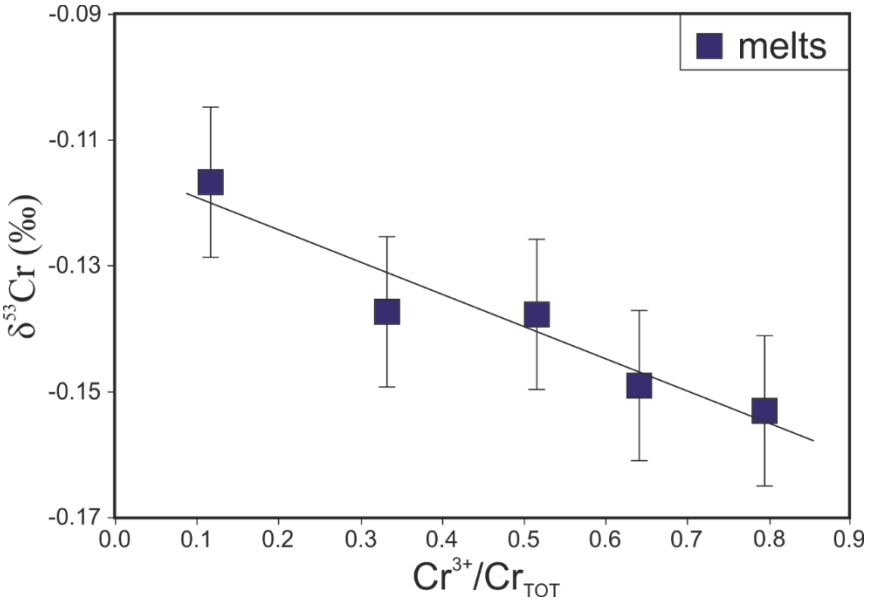
926 **Figure 8**: Partition coefficients $DCr_{chromite\text{-}melt}$ (dark green) and $DCr^{3+}_{chromite\text{-}melt}$ (light green) versus

927 oxygen fugacity. The square and round symbols are series A and B experiments, respectively.



928

929 **Figure 9**: Cr isotopic compositions versus logfO_2 in series A (a) and series B (b) experiments. The red
930 circles are chromite and the blue squares are silicate melts. The grey bar in (a) is the Cr isotopic
931 composition of the chromite used as the starting material in the series A experiments.



932

933 **Figure 10**: Chromium isotopic composition versus the Cr^{3+}/Cr_{TOT} ratio in the series A experiments

934 performed at $\log fO_2 < -6$.

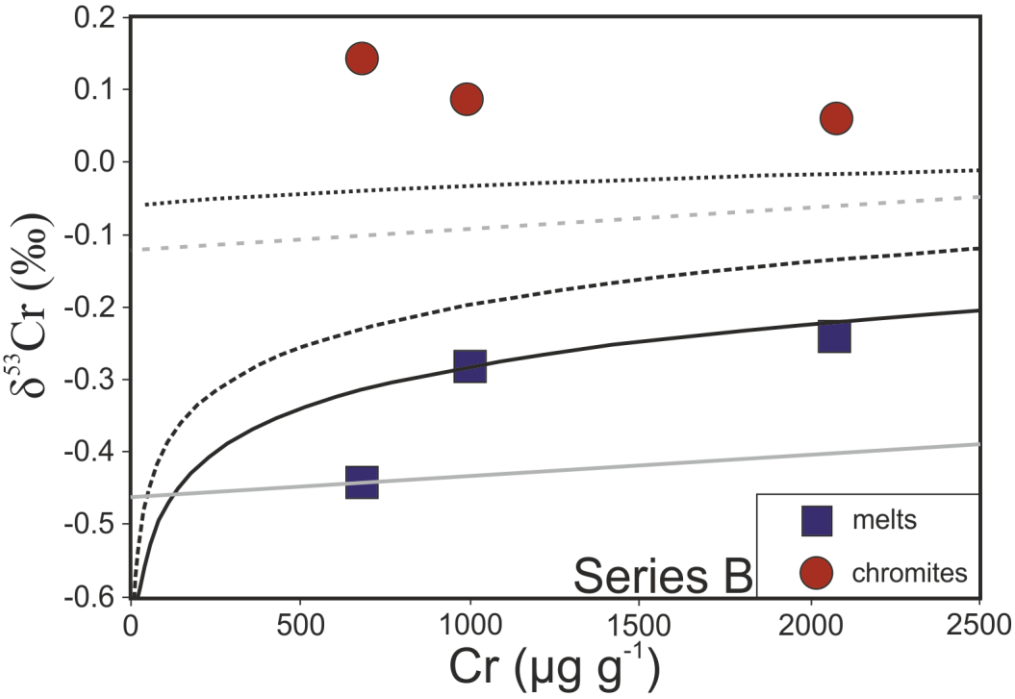
935

936

937

938

939



940

941 **Figure 11**: Chromium isotopic composition of melts and chromite versus Cr concentration for the
942 silicate melts of the series B experiments. The black lines correspond to a Rayleigh fractionation
943 model performed with a fractionation factor of 0.085. The solid black line is the silicate melt isotopic
944 composition. The dashed and dotted black lines are the instantaneous and cumulative chromite
945 isotopic composition, respectively. The grey lines are an equilibrium fractionation model. The solid
946 and dashed grey lines are the silicate melt and chromite isotopic compositions, respectively. For this
947 model, we used $\delta^{53}Cr_{chromite} - \delta^{53}Cr_{melt} = 0.4$ ‰. In both models, the starting Cr concentration is 13500
948 µg g^{-1}.The blue squares and red circles show the isotopic compositions of the coexisting silicate melts
949 and chromite, respectively.

950
951
952
953
954
955
956
957

Table 1: Average chemical composition of the starting silicate melts in series A and B experiments.

Wt. %	Series A	2 s.d.	Series B	2 s.d.
MgO	11.78	0.17	11.74	0.25
Al_2O_3	15.59	0.15	15.39	0.29
SiO_2	47.22	0.31	45.78	0.43
Cr_2O_3	n.d.	n.d.	1.97	0.04
FeO	7.36	0.11	7.41	0.21
CaO	17.58	0.16	17.43	0.45
Total	99.53	0.38	99.72	0.51

983 Table 2: Experimental settings for series A and B experiments.

series A	T (°C)	P (bar)	logfO_2	ΔQFM	Loop	time (hours)
A1	1300	1	-11.9	-4.57	Re	168
A2	1300	1	-9.6	-2.26	Re	168
A3	1300	1	-8.4	-1.09	Pt	168
A4	1300	1	-7.5	-0.13	Pt	168
A5	1300	1	-6.6	0.74	Pt	168
A6	1300	1	-5.8	1.58	Pt	168
A7	1300	1	-3.9	3.40	Pt	168
Time series						time (hours)
A3a	1300	1	-8.4	-1.09	Pt	2
A3b	1300	1	-8.4	-1.09	Pt	24
A3c	1300	1	-8.4	-1.09	Pt	72
A3d	1300	1	-8.4	-1.09	Pt	120
A3	1300	1	-8.4	-1.09	Pt	168
Series B						time (hours)
B1	1300	1	-10.2	-2.86	Pt	168
B2	1300	1	-7.8	-0.46	Pt	168
B3	1300	1	-5.5	1.84	Pt	168

984
985
986
987
988
989
990
991
992
993
994
995
996
997
998
999

Table 3: Major element concentration (wt. %) of the silicate melts in the series A and B experiments

Series A	**MgO**	2 s.d.	**Al_2O_3**	2 s.d.	**SiO_2**	2 s.d.	**Cr_2O_3**	2 s.d.	**FeO**	2 s.d.	**CaO**	2 s.d.	**Total**	2 s.d.	NBO/T	Fe^{3+}/Fe^{2+}	Fe^{3+}/Fe_{TOT}	Cr^{2+}/Cr^{3+}	Cr^{3+}/Cr_{TOT}
A1	11.89	0.15	15.50	0.22	47.30	0.24	0.81	0.04	6.77	0.16	17.52	0.16	99.79	0.41	0.53	0.01	0.01	7.64	0.12
A2	11.76	0.12	15.41	0.08	46.99	0.57	0.28	0.01	7.44	0.12	17.61	0.16	99.49	0.66	0.55	0.03	0.03	2.01	0.33
A3	11.75	0.14	15.50	0.21	47.32	0.22	0.18	0.01	7.34	0.15	17.57	0.13	99.66	0.52	0.54	0.06	0.06	0.95	0.51
A4	11.79	0.08	15.24	0.18	47.34	0.26	0.15	0.01	7.42	0.12	17.49	0.10	99.42	0.28	0.55	0.10	0.09	0.56	0.64
A5	11.61	0.09	15.48	0.11	47.30	0.35	0.12	0.01	7.43	0.09	17.48	0.15	99.41	0.50	0.54	0.17	0.15	0.26	0.79
A6	11.44	0.10	15.36	0.13	46.93	0.26	0.09	0.02	7.66	0.18	17.62	0.08	99.10	0.31	0.55	0.28	0.22	0.00	1.00
A7	11.56	0.07	15.35	0.13	47.20	0.21	0.09	0.02	7.63	0.12	17.54	0.18	99.38	0.18	0.55	0.80	0.44	-0.07	1.07
Time series																			
A3a	11.79	0.10	15.63	0.20	47.20	0.39	0.02	0.03	7.34	0.07	17.64	0.12	99.62	0.53	0.54	0.06	0.06	N/A	N/A
A3b	11.80	0.15	15.59	0.13	47.23	0.26	0.12	0.05	7.37	0.14	17.58	0.13	99.67	0.35	0.54	0.06	0.06	N/A	N/A
A3c	11.79	0.16	15.61	0.12	47.20	0.23	0.16	0.01	7.42	0.08	17.55	0.11	99.72	0.37	0.54	0.06	0.06	N/A	N/A
A3d	11.76	0.25	15.54	0.12	47.24	0.26	0.18	0.02	7.38	0.12	17.52	0.22	99.62	0.26	0.54	0.06	0.06	N/A	N/A
A3	11.75	0.14	15.50	0.21	47.32	0.22	0.18	0.01	7.34	0.15	17.57	0.13	99.66	0.52	0.54	0.06	0.06	1.10	0.48
series B																			
B1	11.62	0.21	15.26	0.17	47.43	0.36	0.30	0.06	6.82	0.18	18.05	0.33	99.57	0.64	0.55	0.02	0.02	2.25	0.31
B2	11.56	0.20	15.21	0.24	47.17	0.41	0.15	0.03	7.38	0.25	17.98	0.28	99.59	0.55	0.56	0.09	0.08	0.57	0.64
B3	11.36	0.34	15.12	0.46	46.84	0.52	0.10	0.03	7.35	0.21	17.83	0.75	99.43	1.67	0.58	0.32	0.24	0.07	0.93

Fe^{3+}/Fe_{TOT} and Fe^{3+}/Fe^{2+} are calculated from O'Neill (2018), Cr^{3+}/Cr_{TOT} and Cr^{2+}/Cr^{3+} are calculated using Hanson and Jones (1998) method. See text for details.

1007 Table 4: Chemical composition of selected chromite (wt. %) in the series A and B experiments. For each experiment, core and rim compositions are reported.

series A		MgO	Al_2O_3	TiO_2	Cr_2O_3	FeO	MnO	Total	Mg#	Cr#	Fe^{3+}#
A1	core	12.11	16.20	0.51	47.41	23.32	0.19	99.8	0.56	0.66	0.09
	rim	17.50	29.00	0.02	43.54	9.89	0.07	100.2	0.76	0.50	0.00
A2	core	13.02	16.10	0.51	47.98	22.04	0.14	99.9	0.60	0.67	0.09
	rim	17.08	27.75	0.01	43.97	10.96	0.04	100.2	0.75	0.52	0.01
A3	core	10.85	15.96	0.50	47.21	25.00	0.23	99.8	0.51	0.67	0.09
	rim	15.50	22.52	0.22	47.81	12.23	0.06	98.9	0.70	0.59	0.01
A4	core	10.82	15.82	0.50	47.59	24.97	0.23	100.0	0.51	0.67	0.09
	rim	16.48	24.87	0.16	45.40	12.72	0.06	100.1	0.73	0.55	0.02
A5	core	12.42	15.99	0.50	48.14	22.85	0.18	100.1	0.57	0.67	0.09
	rim	15.80	19.59	0.40	48.42	15.65	0.10	100.2	0.71	0.62	0.05
A6	core	17.54	16.05	0.50	49.20	16.20	0.08	99.6	0.78	0.67	0.10
	rim	17.95	20.79	0.05	38.98	21.77	0.04	99.8	0.78	0.56	0.17
A7	core	18.22	16.18	0.52	50.20	15.00	0.06	100.2	0.81	0.68	0.10
	rim	18.66	18.16	0.06	39.75	23.17	0.04	100.2	0.80	0.60	0.20
series B											
B1	core	13.85	8.02	0.03	64.91	11.95	0.00	98.7	0.67	0.84	0.00
	rim/small	17.86	27.01	0.00	44.48	9.97	0.06	100.0	0.78	0.53	0.01
B2	core	14.73	13.20	0.01	58.37	12.30	0.06	98.7	0.70	0.75	0.01
	rim/small	17.92	28.06	0.00	42.43	11.75	0.05	100.7	0.78	0.50	0.03
B3	core	14.67	8.36	0.00	62.37	13.80	0.06	99.3	0.71	0.83	0.04
	rim/small	18.20	25.46	0.00	39.12	15.87	0.05	99.2	0.80	0.51	0.10

1008

1009

1010

1011 Table 5: Cr isotopic composition for the silicate melts and the chromite for the series A and B
1012 experiments.

series A	$logfO_2$	$\delta^{53}Cr_{melt}$	2 s.e.	$\delta^{53}Cr_{chromite}$	2 s.e.
A1	-11.9	-0.117	0.006	-0.110	0.006
A2	-9.6	-0.137	0.005	n.d.	n.d.
A3	-8.4	-0.138	0.005	-0.115	0.004
A4	-7.5	-0.149	0.005	n.d.	n.d.
A5	-6.6	-0.153	0.004	n.d.	n.d.
A6	-5.8	-0.449	0.005	-0.102	0.009
A7	-3.9	-0.431	0.005	-0.108	0.009
Time series					
A3a	-8.4	-0.251	0.018	n.d.	n.d.
A3b	-8.4	-0.167	0.007	n.d.	n.d.
A3c	-8.4	-0.147	0.005	n.d.	n.d.
A3d	-8.4	-0.143	0.005	n.d.	n.d.
A3	-8.4	-0.138	0.005	-0.115	0.004
series B					
B1	-10.2	-0.240	0.006	0.063	0.010
B2	-7.8	-0.274	0.006	0.088	0.011
B3	-5.5	-0.437	0.008	0.150	0.008
starting material		-0.060	0.007		
JP-1	N/A	-0.108	0.014*		

1013 * 2 s.d. n=8

1014

1015

1016